APPLICATION OF LAYOUT AND TOPOLOGY OPTIMIZATION USING PATTERN GRADATION FOR THE CONCEPTUAL DESIGN OF BUILDINGS

BY

LAUREN LYNNE STROMBERG

THESIS

Submitted in partial fulfillment of the requirements
for the degree of Master of Science in Civil Engineering
in the Graduate College of the
University of Illinois at Urbana-Champaign, 2010

Urbana, Illinois

Advisor:

Professor Glaucio H. Paulino

Abstract

This work explores the use of manufacturing-type constraints, in particular pattern gradation and repetition, in the context of layout optimization. By placing constraints on the design domain in terms of number and size of repeating patterns along any direction, the conceptual design for buildings is facilitated. To substantiate the potential future applications of this work, examples within the context of high-rise building design are presented. Successful development of such ideas will lead to practical engineering solutions, especially during the building design process. Throughout this work, a continuous topology optimization formulation is utilized with compliance as the objective function and constraints on the pattern geometry. Examples are given to illustrate the ideas developed both in two-dimensional and three-dimensional building configurations.

To my father, **Barry** *and my mother,* **Kathy**.

Acknowledgments

It is a pleasure for me to express my gratitude to all those who have supported me in this work. First and foremost, this thesis would not have been possible without the the help of my adviser, Professor Glaucio H. Paulino. His tremendous energy and excitement about research in general has encouraged me to explore the realm of academia through graduate studies. I owe my deepest gratitude for his impact on my intellectual development and look forward to beginning my PhD under his supervision.

I would also like to thank my student colleagues, especially research group members Kyoungsoo Park, Eshan Dave, Tam Nguyen, Cameron Talischi, Arun Gain, Sofie Leon, Tomas Zegard, Daniel Spring, Rodrigo Espinha, and Ying Yu for their help and support throughout this study. They have provided me with a stimulating work environment, and their ideas and discussions have contributed significantly towards this work. Specifically, I would like to acknowledge Cam Talischi for his suggestions and help editing this thesis.

I have benefited greatly from my experience working with Skidmore, Owings & Merrill (SOM) and am very thankful for the ongoing collaboration. In particular, I would like to acknowledge William Baker, Alessandro Beghini, Juan Carrion and the optimization group for their suggestions on how to make this work more applicable to the structural design world.

Additionally, I am grateful for the financial support provided to me by the National Science Foundation through the Graduate Research Fellowship Program and by the Department of Civil and Environmental Engineering at the University of Illinois at Urbana-Champaign.

I am indebted to Alessandro Beghini for his continued support and encouragement. His

galvanized attitude and insightfulness is a daily source of inspiration for me. I am extremely thankful for the emotional support, camaraderie, entertainment and kindness he has provided throughout this time.

Finally, I wish to thank my family for their support and guidance. It is with pleasure that I dedicate this thesis to my parents for everything they have done for me.

Table of Contents

List of Figures

List of Tables

Nomenclature

$\mathbf{B}$	strain-displacement matrix
c	compliance
$\mathbf{C}^0$	constitutive matrix of solid material
E^0	Young's Modulus of solid material
$\mathbf{f}$	global load vector
J	determinate of Jacobian matrix
$\mathbf{K}$	global stiffness matrix
$\mathbf{K_e}$	element stiffness matrix
$\mathbf{K_e^0}$	stiffness matrix for a solid element
m	number of nodes of the finite element
N_j^e	shape function of node j for element e
n	number of patterns in one direction (x, y, or z)
p	penalization factor for SIMP
Q	number of quadrature points
q	degree of projection weighting function
r_j^e	radius from centroid of element e to node j
r_{min}	minimum radius of projection
r_{max}	maximum radius of projection
$\mathbf{u}$	global displacement vector
$\mathbf{u_e}$	element displacement vector
V	volume
V_s	maximum volume constraint
w_{GP}	weight for quadrature at Gauss point

w_j^e	projection weight of node j of element e
$\mathbf{x}$	location of a point in the domain
x^*	point inside a mapped pattern
$\mathbf{x}_{GP}$	location of a Gauss point
x_n	minimum bound of pattern n in x-direction
x_{n+1}	maximum bound of pattern n in x-direction
y_n	minimum bound of pattern n in y-direction
y_{n+1}	maximum bound of pattern n in y-direction
z_n	minimum bound of pattern n in z-direction
z_{n+1}	maximum bound of pattern n in z-direction
α_n	ratio of pattern n to largest pattern of domain in x-direction
β_n	ratio of pattern n to largest pattern of domain in y-direction
γ_n	ratio of pattern n to largest pattern of domain in z-direction
ν	Poisson's ratio
ρ	density
ρ^*	mapped density
ρ_d	design variable
ρ_e	element density
ρ_j^e	density at node j of element e
ρ_{min}	minimum allowable density
Ω	design domain
Ω_e	domain of element e

List of Abbreviations

2D	Two-Dimensional
3D	Three-Dimensional
AISC	American Institute of Steel Construction
API	Application Programming Interface
CAMD	Continuous Approximation of Material Distribution
ESO	Evolutionary Structural Optimization
FEA	Finite Element Analysis
FEM	Finite Element Method
FGM	Functionally Graded Material
KE	Element Stiffness Matrix
MBB	Messerschmitt-Bölkow-Blohm (Beam)
MEP	Mechanical Electrical Plumbing
MMA	Method of Moving Asymptotes
MTOP	Multiresolution Topology Optimization
OC	Optimality Criteria
SIMP	Solid Isotropic Material with Penalization
TopS	Topological Data Structure

Chapter 1

Introduction

Topology optimization is a relatively new and powerful tool in the field of structural mechanics [Rozvany, 2001]. Currently, its applications span from mechanical engineering to aerospace engineering [Krog et al., 2004, Sigmund, 2000, Carbonari and Paulino, 2009, Schramm et al., 2002]. The ideas presented in this thesis attempt to transition the technology towards the area of structural engineering by exploring the patterns associated with the conceptual design of the bracing systems of buildings. In this chapter, the background information on topology optimization is discussed with a follow-up section on layout optimization and its use of manufacturing constraints. Next, a review of pattern repetition is given and then discussed in the context of the conceptual design of high-rise buildings to motivate a new technique known as pattern gradation. Finally, the organization of this thesis is briefly outlined.

1.1 Background on Topology Optimization

Several optimization techniques have been developed to reduce the expenses associated with structural design by satisfying specific design criteria while using less material. For example, *size optimization* adds or subtracts cross-sectional area from each member where appropriate to satisfy such design criteria. In this method, the shape or connectivity of members may not change, but they may be removed during the process. Size optimization is often used to find the optimal thicknesses of plate elements. An alternative technique, *shape optimization*, looks at the shape of the initial material layout in a design domain and morphs the shape boundaries to obtain an optimal solution. In this case, the optimization can reshape the

material inside the domain, but retains its topological properties such as number of holes [Bendsoe and Sigmund, 2003, Haslinger and Makinen, 2003].

An optimization tool commonly used in the design industry is the use of genetic algorithms, where principles from nature and natural selection can be used to identify the ideal form for a function in a specific landscape (see Gerfen [August 2009]). Though this technique works on a wide range of problems and does not require the use of potentially complicated derivatives, it often requires more function evaluations and is not necessarily convergent, even to local minima [Rozvany, 2008].

To overcome some of the limitations present in the above techniques, topology optimization is introduced. Topology optimization is a mathematical, usually (but not always) gradient-based design tool which determines the location in a design domain to place material based on the loads and boundary conditions for a specific objective (i.e. a target deflection, compliance, etc.). The feasible solutions can have any shape, size or connectivity. In this technique, the finite element method (FEM) is applied by splitting a design domain into several small pieces, known as finite elements. In a topology optimization solution, each element is used to represent the conceptual design in the same fashion as a pixel of an image by containing a density that is either solid (black) or void (white).

1.2 Layout Optimization Issues

The spatial arrangement of material, often known in the literature as the layout problem, is of key importance for the design and usability of many engineering products [Cagan et al., 2002]. *Specifically, in building design, the manner in which material is distributed is significant for engineers to develop a lateral bracing system or create a conceptual design for structural members.*

While topology optimization is a very powerful tool for design, often the resulting topologies produced consist of complex geometries and poor material layouts which are of little value to real-world problems due to expense and ease of manufacturing. An example of a

typical topology optimization result without manufacturing constraints is given in Figure 1.1. Therefore, in order to make the results more significant from an engineering perspective, several constraints can and should be imposed (see Figure 1.1(c) with symmetry and pattern gradation constraints). For example, Guest et al. [2004] proposed a method to limit the minimum member size through a fixed-length scale which was also extended to an integrated scheme which includes both maximum and minimum member control concurrently by means of a penalization factor aimed at providing more control on member sizes Guest [2009]. These methods project the neighboring design variables onto the element density, which also eliminates numerical instabilities such as checkerboarding (patches of alternating black and white material) or mesh dependence (different solutions for different levels of mesh refinement). Similarly, Almeida et al. [2009] developed a method to control the minimum hole size by proposing an inverse projection scheme. The work by Le [2006] implements a minimum length scale to eliminate undesirable patterns in the topological design space by introducing additional layers of design variables. By adapting and applying these technologies for this work, structural engineers can extend topology optimization to design the structural systems of buildings by looking at the constraints on the size and shape of the available materials. Moreover, the minimum member size control has been included in this work to achieve meaningful results.

Alternatively, several sensitivity and density filters have been developed as manufacturing constraints as well. Bourdin [2001] proposed a filtering technique by regularizing the density field through the use of a convolution operator to replace the point-wise element densities. Borrvall and Petersson [2001] also implemented a different density filter through regularized density control. Then, Wang and Wang [2005] developed a bilateral filtering technique to perform checkerboard-free, mesh dependent, edge preserving topology optimization. Similarly, work on sensitivity filters has been done by Sigmund [1997, 2001]. For a discussion on such techniques, the reader may refer to the review paper by Sigmund and Petersson [1998]. Later, Sigmund [2007] proposed density filters using the idea of morphology-based black and white filters to alleviate gray regions between solid and void material which provided

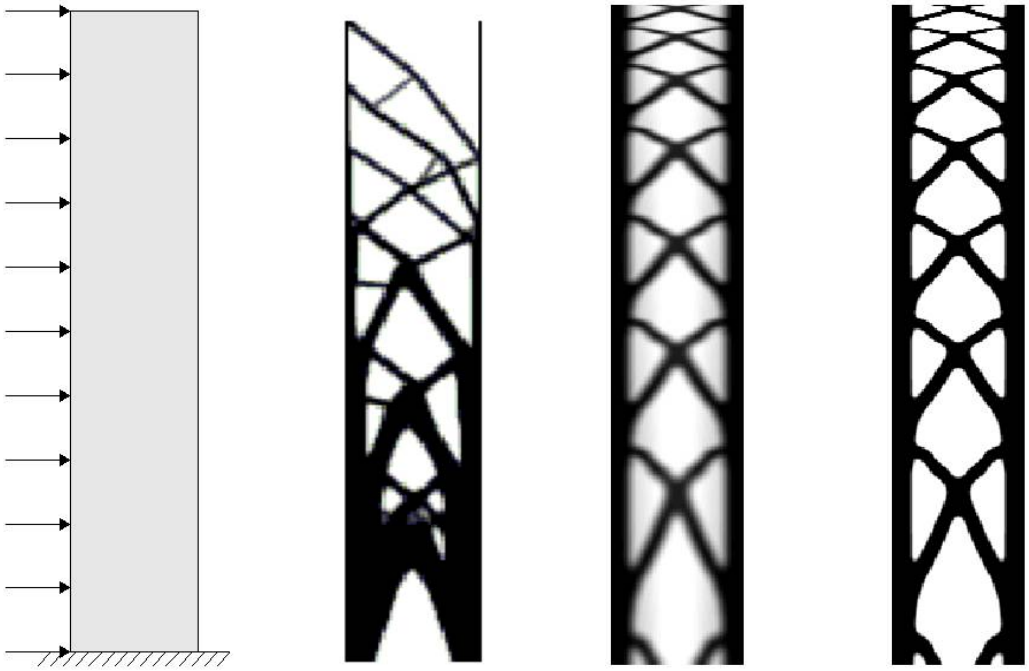

Figure 1.1: Topology optimization design for cantilever: (a) design domain subject to lateral load, (b) without consideration of manufacturing constraints, (c) with pattern gradation and symmetry constraints, (d) proposed design based on interpretation of topology optimization result

control over the minimum member and hole sizes as an additional feature. An alternative to the filtering techniques is the perimeter-control studied by Ambrosio and Buttazzo [1993] and Haber et al. [1996]. The use of a constraint on perimeter-control alleviated the mesh-dependence problem (in addition to the checkerboarding instability as well).

Several other geometrical manufacturing constraints have been developed for application to topology optimization, such as extrusion of a constant cross-section to produce three dimensional structures [Ishii and Aomura, 2004, Zhou et al., 2002]. Moreover, Zuo et al. [2006] added other constraints, including minimum hole size and symmetry to produce more practical designs by incorporating the method of moving asymptotes (MMA) with wavelets. Such techniques may be applicable and relevant for high-rise buildings and could later serve as an extension to this work.

1.3 Pattern Repetition and Gradation

Pattern repetition has been previously implemented in topology optimization for a variety of problems. Almeida et al. [2010] developed manufacturing constraints, specifically pattern repetition and symmetry, to functionally graded materials (FGMs) on both a global and local scale. Huang and Xie [2008] used the bidirectional evolutionary structural optimization (ESO) to come up with the optimal designs of periodic structures by splitting the design domains into unit cells that are constrained to have the same material layouts. However, it has been shown that often times ESO methods can produce nonoptimal solutions [Zhou and Rozvany, 2001].

Other work has been done using periodicity, or pattern repetition, for the design of microstructures. Paulino et al. [2009] developed a material design method which combines topology optimization with homogenization to design periodic functionally graded composites. In Qiu et al. [2009] the effects of 2D periodic repetition and cyclic-symmetry for cellular structures were studied using super-elements and perimeter control. Also topology optimization has been applied to periodic microstructures in electromagnetic material for wave propagation [Nomura et al., 2009] and for lightweight cellular materials [Zhang and Sun, 2006]. However, rather than looking at a small scale, this work proposes the application of pattern repetition to a larger scale for the conceptual design of buildings. Additionally, in modern architecture often times patterns are asymmetric to account for layout and space considerations or aesthetic value.

Furthermore, the next logical step is to extend the concept of pattern repetition, or periodic structures, by changing the size and shape of the patterns. In this work, this concept is described as pattern gradation. By geometrically grading such repeating patterns in a structure, or more specifically in a building, it is possible for structural engineers to come up with a conceptual design for the optimal lateral bracing systems and/or the optimal angles for the diagonal bracing to follow. Moreover, by optimizing the structural system, the consumption of resources would be reduced. According to the manual for Leadership

in Energy and Environmental Design (LEED®) [U.S, 2005], buildings currently account for one-third of our total energy, two-thirds of our electricity, and one-eighth of our water supply. In addition, the current standard in the construction industry for sustainable design [U.S, 2005] acknowledges under the category "Innovation & design process" that a new building, which shows a significant reduction in the use of materials would be awarded up to 4 points in the rating system. By optimizing the amount of natural resources used, such green buildings potentially may impact public health and the environment, reduce operating expenses and create a sustainable community.

1.4 On Application of Manufacturing Constraints to Buildings

Manufacturing constraints in topology optimization are relevant and necessary to extend the current solutions to the structural engineering industry. For instance, manufacturing constraints can be imposed on the minimum and maximum member sizes for topology optimization designs in accordance with the available minimum and maximum sizes in the American Institute of Steel Construction (AISC) specifications for steel shapes [Ame, 2005]. Within these shapes, a designer must check the limit states associated with each member. Thus, a constraint on the allowable stress levels can be imposed as well.

With respect to the dynamic analysis of a structure, it may be valuable to target a certain frequency by means of a period optimization. For example, typically the first period for a building should be the longitudinal period as opposed to the torsional period since the torsional period discomforts occupants the most. Moreover, some design codes (such as the Chinese design codes Min [2003, 2002]) enforce that the ratio of the longitudinal and torsional periods must be higher than a certain value. This situation introduces the necessity for manufacturing constraints on the periods of a structure.

In the design phase of a building, for example, one may need to run a pipe through a beam to integrate the structural system with the mechanical electrical and plumbing (MEP) systems. A manufacturing constraint on a minimum or maximum hole size in a domain could

be applied in this situation to create a conceptual design for the beam which incorporates space for such a hole.

Furthermore in regards to the glass curtain wall of a high-rise building, custom cut glass shapes typically result in very costly designs. A manufacturing constraint on the exterior cladding will decrease the need for special shapes. Here, pattern repetition is imposed so glass shapes can be cut in the same fashion and panels are repeated throughout the height of the structure.

For the structural system of a concrete building, formwork is manufactured to pour each component. With a manufacturing constraint on pattern repetition, the formwork can be reused from floor to floor, increasing the speed with which the building can be constructed. In the case of a steel building with pattern repetition, the same connections can be used throughout the height of the building. By repeating the same connections, the cost can be lowered and the quality control of such connections is increased.

The need for a manufacturing constraint on the geometric pattern gradation, or the stretching and shrinking of patterns along the height of a building, becomes very clear when by considering the structural members of a building. Under typical loading conditions, the columns of a building will always be larger in size at its base and smaller towards the top. We introduce the pattern gradation constraint as an effective means to smoothly transition the design from one extreme to another. This concept can be further explored in the context of bracing angles. For example, the lateral design at the top of a high-rise building is controlled by shear loads and the optimal bracing angle is 45 degrees. However, buildings typically suffer from overturning moments, due to wind loads, near the base. Here the bracing angle should be much larger in the range of 65-70 degrees [Moon et al., 2007]. Again, the patterns from the base to the top of the building will transition from having a 70 to 75 degree angle to a 45 degree angle.

In addition to transitioning, the pattern gradation can also be applicable in the context of constraints on the height of a floor. For instances where a certain level in a building might need to be taller to house the mechanical equipment, the gradation can be used to maintain

the structural integrity and aesthetics while slightly adjusting the size and capacity of the members.

Finally, we motivate this work to aid the conceptual design process of a structure by introducing manufacturing constraints in the context of layout optimization, with an emphasis placed on the pattern gradation constraint as an application for high-rise buildings.

1.5 Thesis Organization

This thesis is organized as follows: the background information of the topology optimization is discussed in Chapter 2 and then this formulation is extended to include the effects of pattern repetition and gradation for two methods in Chapter 3. Next, the computational implementation in Matlab® for the current work is described in Chapter 4 and some pseudo-code is provided. Following in Chapter 5 are the numerical results obtained for both 2D and 3D problems, with some applications to high-rise building design. Finally, a summary and conclusion are given with suggestions for the extension of this work in the future.

Chapter 2

Background Information

In this chapter, the background information pertaining to the topology optimization formulation and finite element (FE) framework is discussed, including the governing equations, different approaches and methodologies used in this work. Additionally, the implementation aspects are included with a description of the multiresolution topology optimization (MTOP) approach and its advantages for modeling large scale structures such as high-rise buildings.

2.1 Topology Optimization Framework

Topology optimization consists of searching for the optimal layout of material in a given design domain in terms of an objective function. Throughout this thesis, the aim is to maximize the stiffness of the structure (i.e. building in most of the examples presented). The minimum compliance problem can be stated in terms of the density, ρ, and the displacements, $\mathbf{u}$, as follows:

$$\begin{aligned} \min_{\rho,\mathbf{u}} \quad & c(\rho,\mathbf{u}) \\ s.t. \quad & \mathbf{K}(\rho)\mathbf{u} = \mathbf{f} \\ & \int_{\Omega} \rho \, dV \leq V_s \\ & \rho(\mathbf{x}) \in [0,1] \, \forall \, \mathbf{x} \in \Omega \end{aligned} \tag{2.1}$$

The compliance of the structure is denoted by c, $\mathbf{K}(\rho)$ represents the global stiffness matrix, which depends on the material densities, while $\mathbf{u}$ and $\mathbf{f}$ are the vectors of nodal displace-

ments and forces, respectively. The volume constraint, V_s, represents the maximum volume permitted for the design of the structure. The design, or topology of the solution, is determined by the material density, ρ: a zero density value signifies a void whereas one represents solid material.

It is well-known that the topology optimization problem presented here is ill-posed, or lacks a solution in the continuum setting [Peterson and Sigmund, 1998, Kohn and Strang, 1986a,b,c]. Thus, by applying relaxation to allow continuous variation of density in the range $[\rho_{min}, 1]$ rather than restricting each density to an integer value of 0 or 1 the existence of a solution is guaranteed. Here, ρ_{min} is a small parameter greater than zero specified to avoid singularities of the global stiffness matrix, $\mathbf{K}(\rho)$.

For example, the Solid Isotropic Material with Penalization (SIMP) [Rovzany et al., 1992, Zhou and Rovzany, 1991, Bendsoe, 1989, Bendsoe and Sigmund, 1999] model expresses the stiffness for each element as a function of the density using the following well-known power-law relationship:

$$\mathbf{E}(\mathbf{x}) = \rho(\mathbf{x})^p E^0 \tag{2.2}$$

where E^0 describes the Young's modulus of the solid material and p is a penalization parameter with $p \geq 1$. Here, the material properties are continuously dependent on the amount of material at each point. By penalizing the densities, the stiffness for any $\rho < 1$ is small compared to its contribution toward the volume, leading the density towards 0 or 1 rather than remaining in the intermediate range. Moreover, the overall optimization is influenced towards the desired solid-void design and the discrete nature of the design can be recovered.

2.2 Finite Elements for Topology Optimization

The element type used for the finite element analysis in this work is a standard bilinear 4-node quadrilateral (Q4) or 8-node brick (B8) which is computationally more efficient than higher order elements. However, a common concern associated with the Q4 and B8 elements are the appearance of checkerboarding, a numerical phenomenon of alternating regions of

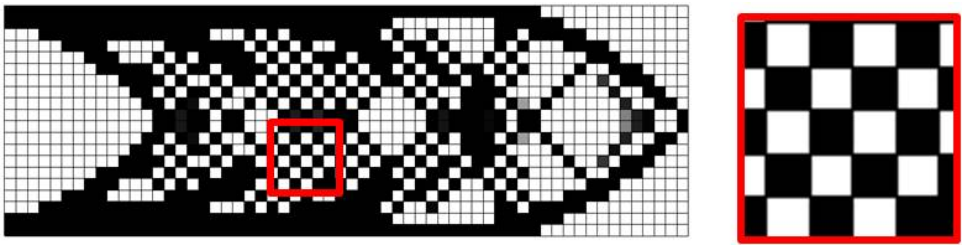

Figure 2.1: Example of "checkerboarding" phenomenon for Q4 elements in FE mesh for topology optimization

solid and void material present in the topology optimization designs (see Figure 2.1). Since the checkerboarding phenomenon overestimates the stiffness of a region or patch of elements, these patches are numerically advantageous and tend to appear frequently in topology optimization. To overcome this problem, a higher order element, such as a Q8 or Q9 could be employed for small penalization parameters with SIMP (see Jog and Haber [1996], Diaz and Sigmund [1995]); however, there is a significant increase in the computational time due to the higher number of degrees of freedom associated with these elements.

As an alternate solution for checkerboarding, additional manufacturing constraints could also be applied such as a filter, where the density or sensitivity is computed as a weighted average of the element and its closest neighbors. However, filters typically suffer from mesh dependence, or the incidence of obtaining different solutions for different discretizations of the FE mesh. A mesh-independent projection scheme with a fixed length scale can also be imposed in this work where the Q4 element is used in combination with a projection method in a similar manner to Guest et al. [2004] and Almeida et al. [2009].

For the pattern gradation two distinct formulations are used: the element-based approach where material is constant throughout each finite element and design variables are located at the element centroids or nodes (nodal design variable approach), and the CAMD approach, where material is approximated by a continuous field. These approaches are described in detail in what follows.

2.2.1 Element-Based Approach

In the uniform element density formulation, each finite element contains one design variable, ρ_e, which represents a constant material density throughout the element. The element stiffness matrix can be expressed in the 2D parent domain as:

$$\mathbf{K}_e = \int_{\Omega_e} \mathbf{B}^T \mathbf{C} \mathbf{B} \, dA = \int_{-1}^{1} \int_{-1}^{1} \mathbf{B}^T (\rho_e^p \mathbf{C}^0) \mathbf{B} J \, d\xi d\eta \tag{2.3}$$

where $\mathbf{B}$ is the strain-displacement matrix, $\mathbf{C}^0$ is the constitutive matrix of the solid material, ξ and η are the natural coordinates, and J is the determinate of the Jacobian matrix. Assuming a state of plane-stress, $\mathbf{C}^0$ is given in terms of the Young's Modulus for solid material, E^0, and Poisson's ratio, ν, as

$$\mathbf{C}^0 = \frac{E^0}{1-\nu^2} \begin{bmatrix} 1 & \nu & 0 \\ \nu & 1 & 0 \\ 0 & 0 & \frac{1-\nu}{2} \end{bmatrix} \tag{2.4}$$

For the 3D parent domain, the equations are instead given as:

$$\mathbf{K}_e = \int_{\Omega_e} \mathbf{B}^T \mathbf{C} \mathbf{B} \, dV = \int_{-1}^{1} \int_{-1}^{1} \int_{-1}^{1} \mathbf{B}^T (\rho_e^p \mathbf{C}^0) \mathbf{B} J \, d\xi d\eta d\zeta \tag{2.5}$$

and

$$\mathbf{C}^0 = \frac{E^0}{(1+\nu)(1-2\nu)} \begin{bmatrix} 1-\nu & \nu & \nu & 0 & 0 & 0 \\ \nu & 1-\nu & \nu & 0 & 0 & 0 \\ \nu & \nu & 1-\nu & 0 & 0 & 0 \\ 0 & 0 & 0 & \frac{1}{2}-\nu & 0 & 0 \\ 0 & 0 & 0 & 0 & \frac{1}{2}-\nu & 0 \\ 0 & 0 & 0 & 0 & 0 & \frac{1}{2}-\nu \end{bmatrix} \tag{2.6}$$

In expression (2.3) or (2.5), the material density of each element can be collected out of the integrand as follows:

$$\mathbf{K}_e = \rho_e^p \int_{-1}^{1}\int_{-1}^{1} \mathbf{B}^T\mathbf{C}^0\mathbf{B}J\, d\xi d\eta = \rho_e^p \mathbf{K}_e^0 \tag{2.7}$$

or for 3D

$$\mathbf{K}_e = \rho_e^p \int_{-1}^{1}\int_{-1}^{1}\int_{-1}^{1} \mathbf{B}^T\mathbf{C}^0\mathbf{B}J\, d\xi d\eta d\zeta = \rho_e^p \mathbf{K}_e^0 \tag{2.8}$$

where $\mathbf{K}_e^0$ represents the stiffness matrix for a solid element.

For the element-based approach, the objective function is the compliance, c, which is defined as

$$c = \mathbf{f}^T\mathbf{u} \tag{2.9}$$

This scalar function is discretized for the optimization as:

$$c = \sum_e \mathbf{u}_e^T \left(\rho_e^p\, \mathbf{K}_e\right) \mathbf{u}_e \tag{2.10}$$

where e denotes each element in the domain. Accordingly, the sensitivity of the compliance can be computed with respect to each element as:

$$\frac{\partial c}{\partial \rho_e} = -\mathbf{u}_e^T \frac{\partial \mathbf{K}_e}{\partial \rho_e}\mathbf{u}_e = -p\rho_e^{p-1}\mathbf{u}_e^T\mathbf{K}_e^0\mathbf{u}_e \tag{2.11}$$

Similarly, the sensitivities of the volume constraint are computed as:

$$\frac{\partial V}{\partial \rho_e} = \int_{\Omega_e} dV = V(\Omega_e) \tag{2.12}$$

2.2.2 Continuous Approximation of Material Distribution

An alternative method to the element-based approach is the Continuous Approximation of Material Distribution (CAMD) [Matsui and Terada, 2004, Rahmatalla and Swan, 2004]. This method uses a continuous material density field over the entire domain in a similar fashion to the displacement field for FEM (see Figure 2.2). Accordingly, the material density at

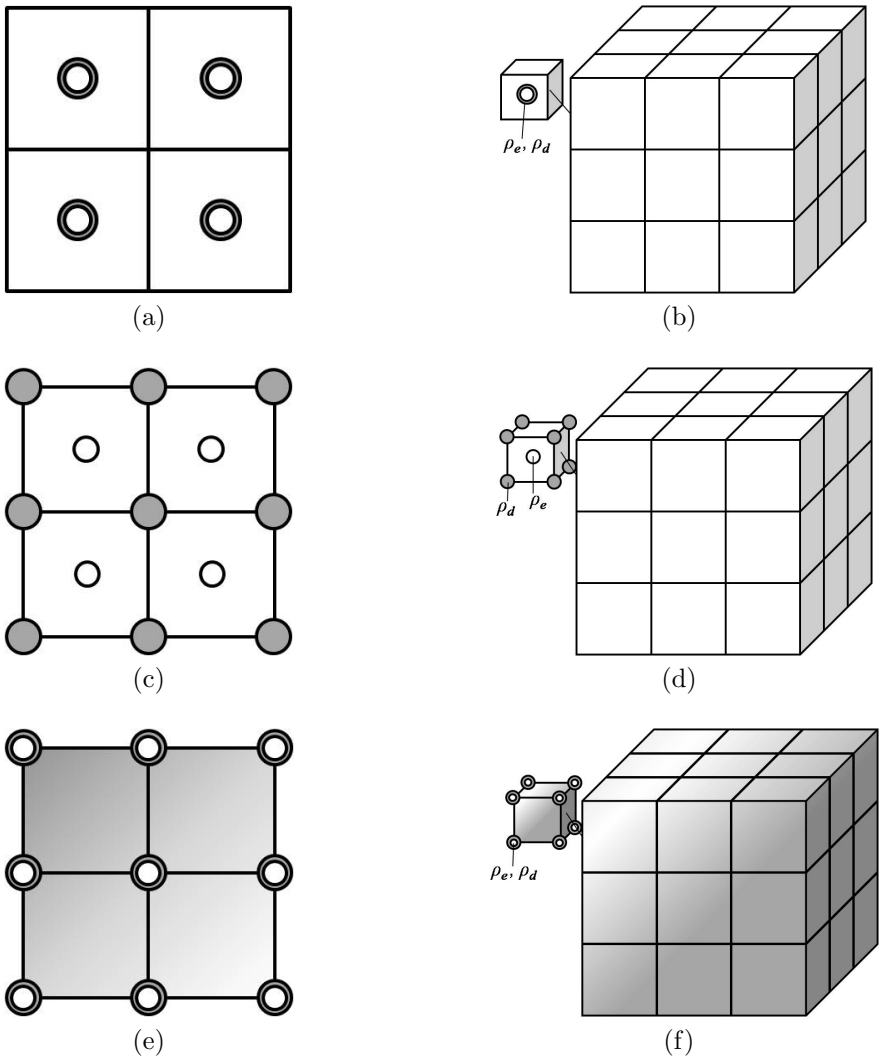

Figure 2.2: An illustration representing the different 2D/3D element types: (a),(b) uniform element densities with design variables at the centroid, (c),(d) uniform element densities with design variables at the nodes, (e),(f) element with continuous material density field (CAMD). Larger gray circles represent the design variables while smaller white circles are the element densities

a point $\mathbf{x}$ inside the finite element is computed through an interpolation scheme using the shape functions N_j^e, given by Matsui and Terada [2004] as:

$$\rho(\mathbf{x}) = \sum_{j=1}^{m} N_j^e(\mathbf{x})\rho_j^e \tag{2.13}$$

where the nodal densities become the design variables. In the expression above, N_j^e is the shape function for node j of element e evaluated at the desired point, $\mathbf{x}$, and ρ_j^e is the corresponding density at node j for element e, and m is the number of nodes of the finite element (i.e. $m = 4$ for a Q4 or $m = 8$ for a B8 element).

The compliance and sensitivity calculated in the previous section must now be modified for the CAMD implementation. The sensitivities can be computed with respect to the nodal densities as:

$$\frac{\partial c}{\partial \rho_j} = -\sum_{e \in \Omega_j} \mathbf{u}_e^T \frac{\partial \mathbf{K_e}}{\partial \rho_j} \mathbf{u}_e \tag{2.14}$$

where Ω_j is given as the domain of neighboring elements that share node j. Similar to the element-based approach previously described, the element stiffness matrix can be defined as

$$\mathbf{K}_e = \int_{\Omega_e} \mathbf{B}^T\mathbf{C}\mathbf{B}\, dA = \int_{\Omega_e} \mathbf{B}^T(\rho^p\mathbf{C}^0)\mathbf{B}\, dA = \int_{-1}^{1}\int_{-1}^{1} \left(\sum_{i=1}^{m} N_i^e(\mathbf{x})\rho_i^e\right)^p \mathbf{B}^T\mathbf{C}^0\mathbf{B}J\, d\xi d\eta \tag{2.15}$$

or for 3D,

$$\mathbf{K}_e = \int_{\Omega_e} \mathbf{B}^T\mathbf{C}\mathbf{B}\, dV = \int_{\Omega_e} \mathbf{B}^T(\rho^p\mathbf{C}^0)\mathbf{B}\, dV = \int_{-1}^{1}\int_{-1}^{1}\int_{-1}^{1} \left(\sum_{i=1}^{m} N_i^e(\mathbf{x})\rho_i^e\right)^p \mathbf{B}^T\mathbf{C}^0\mathbf{B}J\, d\xi d\eta d\zeta \tag{2.16}$$

Expressions (2.15) and (2.16) differ from (2.7) and (2.8) in the way the element densities are treated according to Equation (2.13). To perform the numerical integration, Equation (2.15), or (2.16), are rewritten using a Gaussian quadrature rule with Q points as

$$\mathbf{K}_e = \sum_{GP=1}^{Q} w_{GP} \left(\sum_{i=1}^{m} N_i^e(\mathbf{x}_{GP})\rho_i^e\right)^p \mathbf{B}^T(\mathbf{x}_{GP})\mathbf{C}^0\mathbf{B}(\mathbf{x}_{GP})J \tag{2.17}$$

where $\mathbf{x}_{GP}$ and w_{GP} represent the location and weight respectively of each integration point. Now, using (2.3) to compute the sensitivities for the optimization, the sensitivity of the stiffness matrix with respect to the nodal densities is written as

$$\frac{\partial \mathbf{K}_e}{\partial \rho_j^e} = \int_{-1}^{1}\int_{-1}^{1} pN_j^e \left(\sum_{i=1}^{m} N_i^e \rho_i^e\right)^{p-1} \mathbf{B}^T\mathbf{C}^0\mathbf{B}J \; d\xi d\eta \tag{2.18}$$

or for 3D

$$\frac{\partial \mathbf{K}_e}{\partial \rho_j^e} = \int_{-1}^{1}\int_{-1}^{1}\int_{-1}^{1} pN_j^e \left(\sum_{i=1}^{m} N_i^e \rho_i^e\right)^{p-1} \mathbf{B}^T\mathbf{C}^0\mathbf{B}J \; d\xi d\eta d\zeta \tag{2.19}$$

Equations (2.18) and (2.19) can be expressed in terms of numerical integration as:

$$\frac{\partial \mathbf{K}_e}{\partial \rho_j^e} = \sum_{GP=1}^{Q} pN_j^e(\mathbf{x}_{GP})(\rho_e^{GP})^{p-1}\mathbf{K}_e^{GP} \tag{2.20}$$

where $N_j^e(\mathbf{x}_{GP})$ is the shape function for node j of element e located at the Gauss point GP, and $\mathbf{K}_e^{GP}$ is the integrand computed at point GP. The volume associated with the CAMD problem formulation is computed by integrating all the densities over the design domain given by

$$V = \int_\Omega \rho dV = \sum_e \int_{\Omega_e} \left(\sum_{j=1}^{m} \rho_j^e N_j^e\right) dV = \sum_e \sum_{j=1}^{m} \int_{\Omega_e} \rho_j^e N_j^e dV \tag{2.21}$$

so the sensitivity of the volume is computed as

$$\frac{\partial V}{\partial \rho_j^e} = \sum_{e\in\Omega_j} \int_{\Omega_e} N_j^e dV \tag{2.22}$$

where Ω_j is the set of elements which share node j. Equation (2.21) is numerically evaluated using a Gaussian quadrature rule as:

$$\frac{\partial V}{\partial \rho_j^e} = \sum_{e\in\Omega_j} \sum_{GP=1}^{m} w_{GP} N_j^e(\mathbf{x}_{GP}) \tag{2.23}$$

The CAMD element formulation is suggested here as an alternative to the element-based approach to obtain a smoother gradation. The element-based approach uses piecewise con-

stant functions to model the densities over the finite element, while the CAMD models the densities using the shape functions so the densities vary within each element. Naturally, the concept of graded structures using the generalized isoparametric formulation [Kim and Paulino, 2002] can be applied since the densities are computed using the shape functions for this approach. The CAMD formulation will be revisited in the following chapter and discussed in more detail with an application to pattern gradation.

2.3 Projection Scheme

To avoid checkerboarding or other numerical instabilities (known as "islanding" and "layering"), a projection scheme using a fixed length scale is implemented. According to Guest et al. [2004] and Almeida et al. [2009], the density of each element is computed by taking a weighted average of the neighboring design variables which lie inside the region, Ω_e. This region, Ω_e is selected as the space enclosed by a fixed physical radius, r_{min} in any direction from the centroid of element e that is independent of the mesh. The density of element e is then assigned by projecting a uniform density computed from the neighboring nodal densities.

Even though various weighting functions can be used, this work explores a linear projection scheme ($q = 1$). For this case, the weighting function can be described by a conic section centered about the element centroid, with unit height and base of $2r_{min}$, where r_{min} is the mesh-independent fixed length scale. Accordingly, the weights corresponding to this scheme are given by

$$w_j^e = \begin{cases} \left(1 - \frac{r_j^e}{r_{min}}\right)^q & r \leq r_{min} \\ 0 & r > r_{min}. \end{cases} \tag{2.24}$$

where w_j^e is the weight for node j of element e, r_j^e denotes the length from the element which we are computing the density to the element centroid (or node) that lies in the domain of

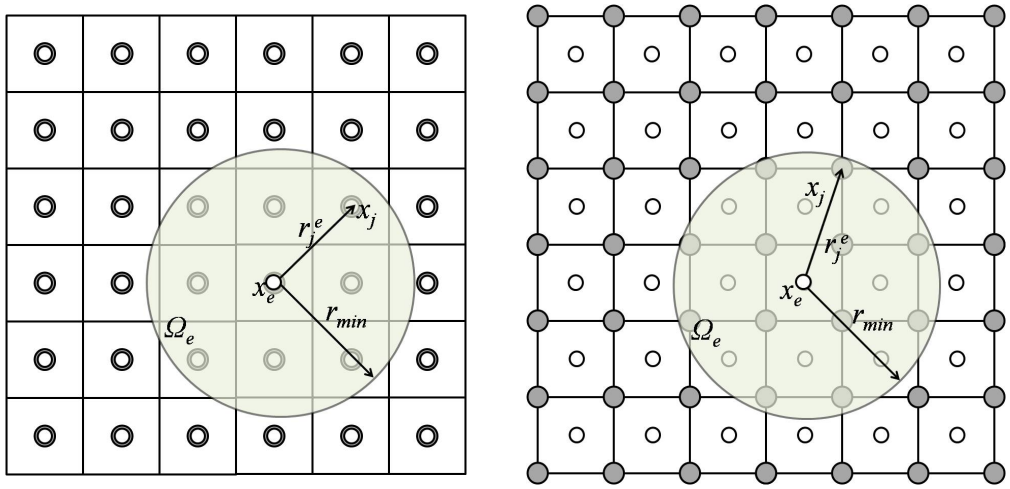

Figure 2.3: Projection scheme for uniform elements with design variables at centroids (a) and nodes (b)

influence, Ω_e. For each element the density is then taken as the weighted average

$$\rho_e = \frac{\sum_{j \in \Omega_e} w_j^e \rho_j^e}{\sum_{j \in \Omega_e} w_j^e} \tag{2.25}$$

Since the element densities are computed as a function of the nodal design variables, the sensitivities must be modified as

$$\frac{\partial c}{\partial \rho_j^e} = \frac{\partial c}{\partial \rho_e} \frac{\partial \rho_e}{\partial \rho_j} = \frac{\partial c}{\partial \rho_e} \left(\frac{w_j^e}{\sum_{j \in \Omega_e} w_j^e} \right) \tag{2.26}$$

By using the projection method above, all of the members in the resulting design are indirectly forced to be larger than the dimension r_{min} so the optimal solutions become more reasonable to manufacture from an industrial standpoint.

If a constraint on the maximum member size were of interest, the fixed length scale r_{max} [Guest, 2009] could be employed by adding a constraint to specify the minimum allowed volume of voids in any particular test region. Moreover, the minimum and maximum member size constraints may be coupled by imposing both constraints for the minimum and maximum volume of voids to give designers more control over manufacturability and cost. As an alternative approach, [Almeida et al., 2009] considers an inverse projection scheme to enforce a minimum hole size in the final topology. For the inverse projection, the element densities

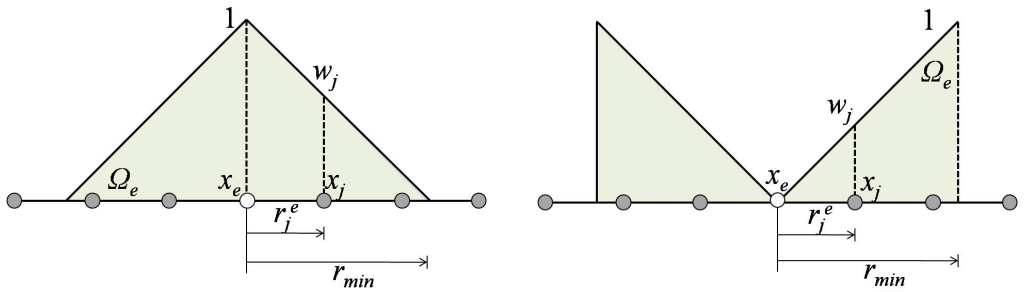

Figure 2.4: Illustration of two different weighting functions for the projection scheme: (a) linear, (b) inverse

are computed using the weights given by

$$w_j^e = \left(\frac{r_j^e}{r_{min}}\right)^q, \quad r \leq r_{min} \tag{2.27}$$

as displayed in Figure 2.3. Using this scheme, both the minimum hole size and the minimum member size must be of at least radius r_{min}.

One more important point to consider is that for either of the direct or inverse projections presented, the weighting function does not necessarily have to be linear as shown. Alternate power-law weighting functions, such as parabolic, cubic, etc. can be generated by raising the expressions given in Equations (2.24) and (2.27) to the power $q > 1$. Additionally, other forms of weighting functions (sinusoidal, exponential, logarithmic, etc.) for the projection scheme could be explored.

2.4 Multiresolution Topology Optimization Implementation

The work presented here includes the multiresolution topology optimization (MTOP) implementation by Nguyen et al. [2010] where each finite element of the displacement mesh contains several density elements. This implementation allows high-resolution designs without increasing the computational cost. In MTOP, three distinct meshes are superimposed: the displacement mesh for the finite element analysis, the density mesh to represent the material distribution over the domain, and the design variable mesh to perform the opti-

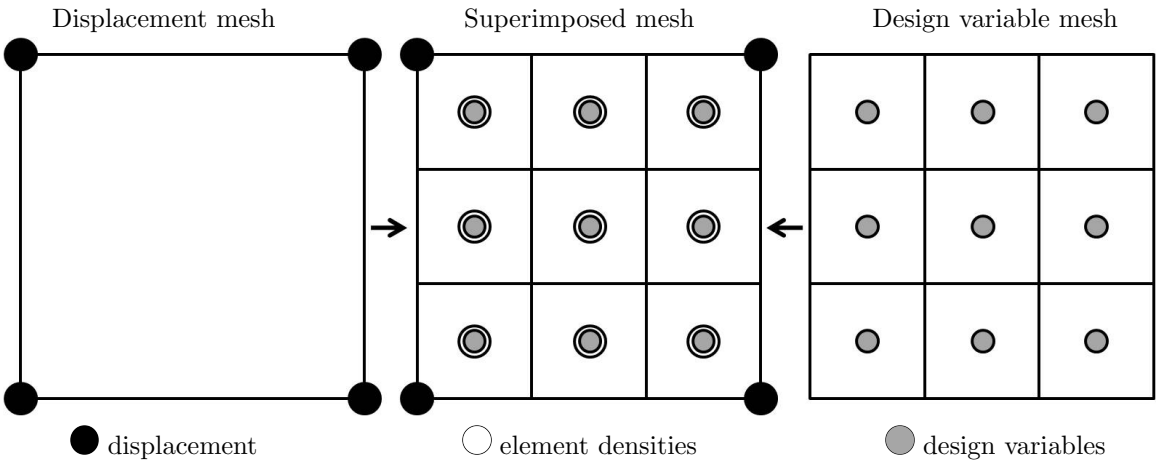

Figure 2.5: Sample Q4/n9 MTOP element

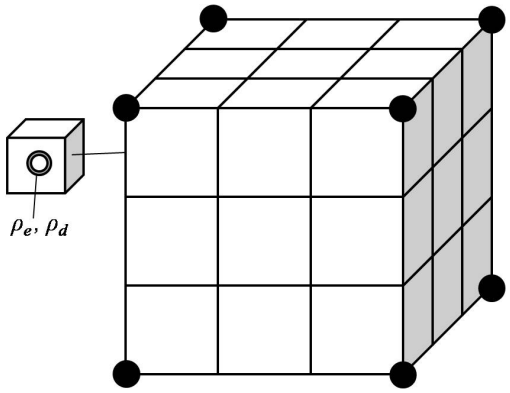

Figure 2.6: Sample B8/n27 MTOP element

mization. The design variable mesh is distinct from the density mesh since the density of each element is computed using the projection scheme described in Section 2.3 by projecting a region of design variables onto each element density. Then, the resulting element densities are used in the computation of the element stiffness matrices and sensitivities.

The current bottleneck in topology optimization problems is the finite element analysis since a large number of progressively ill-conditioned linear systems must be solved for the equilibrium equation, $\mathbf{Ku} = \mathbf{f}$. Thus, by placing several design variable and element densities within each finite element of the coarse mesh (in which the displacements are computed), the time spent on the finite element analysis (FEA) can be reduced (see Figure 2.5 for 2D or Figure 2.6 for the 3D case). This technique accommodates large-scale problems and leads to high-resolution results in a reasonable CPU time.

A few modifications need to be made to account for this multilevel scheme. The stiffness matrix used is computed in the same manner as in the previous cases where ρ_e refers to the density at each displacement element for both the element-based and CAMD approaches. However, for the element based approach since each displacement element contains several densities, these densities must be averaged to obtain ρ_e. For the CAMD approach, the density is computed using the density at the Gauss points and the interpolation in Equation (2.13).

Similarly, the projection method is implemented with the same weighting functions as described in Section 2.3. To obtain the high-quality designs, the design variable mesh should be projected onto the density mesh where the densities are located either at the element centroids or nodes. Additionally, when calculating the sensitivities, the chain rule must be applied to account for the projection as stated previously in Equation (2.26) and the sensitivity of the compliance for each element remains the same as Equation (2.11) where $\mathbf{K}_e$ is computed using the coarse displacement mesh and ρ_e is the element density computed from the projection of the fine mesh of design variables onto the fine density mesh.

Some issues arise concerning the integration of the stiffness matrix. Since MTOP elements are used in this work, a study was conducted to determine whether or not the results would benefit from using a higher-order integration. Because each element contains several density elements which are used to compute the element stiffness matrix, it could be more accurate to use more quadrature points. For an MTOP element with 25 design variables and densities per displacement element, denoted as Q4/n25, it might be beneficial to use a 5 x 5 quadrature rule as opposed to the usual 2 x 2 rule. The optimization of a half-MBB beam was carried out as shown in Figure 2.7 with varied Gauss quadrature rules for the same resolution meshes. The compliance values are given for the respective rules. Here, the FEA is performed on a mesh of 60 x 20 elements with a 240 x 80 design variable mesh, or 16 design variables and densities per Q4 displacement element (MTOP Q4/n16 elements) as shown in Figure 2.7(b). The results presented here prove that 2 x 2 Gaussian integration is satisfactory, since the computed sensitivities and objective functions are essentially the same (see Table 2.1).

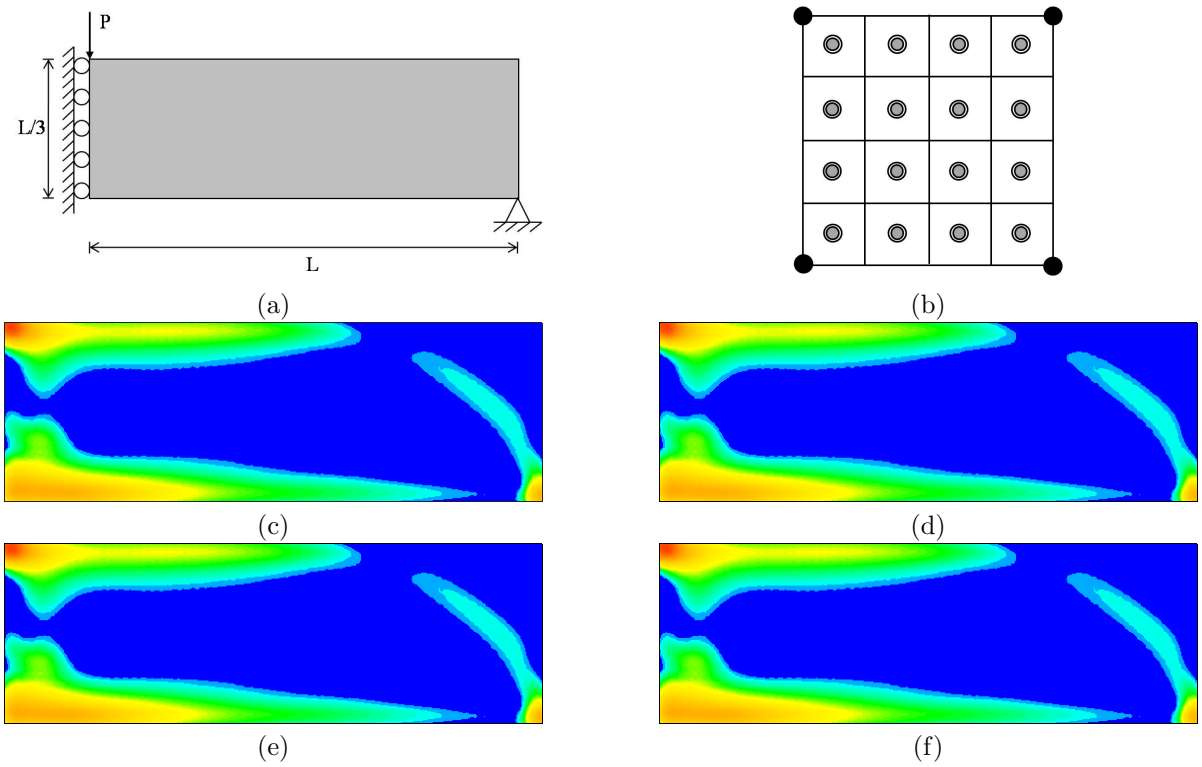

Figure 2.7: Comparison of sensitivities for different orders of integration for MBB Beam discretized with Q4/n16 elements: 60 x 20 element densities with 240 x 80 design variables. Order of Gauss quadrature: (a) 2, (b) 3, (c) 4, and (d) 5

Table 2.1: Values of Compliance for Different Orders of Integration for CAMD MTOP Elements

Element Density Mesh	Order of Quadrature	Compliance
30 x 10	2	209.9062
30 x 10	3	209.8951
30 x 10	4	209.8948
30 x 10	5	209.8948
48 x 16	2	210.7241
48 x 16	3	210.7186
48 x 16	4	210.7186
48 x 16	5	210.7185
60 x 20	2	211.2914
60 x 20	3	211.2902
60 x 20	4	211.2902
60 x 20	5	211.2902
120 x 40	2	213.4746
120 x 40	3	213.4745
120 x 40	4	213.4745
120 x 40	5	213.4745
240 x 80	2	215.8331
240 x 80	3	215.8331
240 x 80	4	215.8331
240 x 80	5	215.8331

To validate the MTOP approach for this work, the effect of varying the levels of refinement of the FEM mesh versus the design variable mesh were studied for a constant order of Gauss quadrature. The results are presented in Table 2.2. As expected, as the finite element mesh is refined for a constant design variable mesh, monotonic convergence is observed. Moreover, this sensitivity analysis shows similar results for a refinement level of 16 design variables per finite element as three finite elements per design variable.

Table 2.2: Values of Compliance for Different Levels of Refinement of FEM Meshes for CAMD MTOP Elements

Design Variable Mesh	Element Density Mesh	Compliance
240 x 80	30 x 10	209.9062
240 x 80	48 x 16	210.7241
240 x 80	60 x 20	211.2914
240 x 80	120 x 40	213.4746
240 x 80	240 x 80	215.8331
240 x 80	480 x 160	218.2252
240 x 80	720 x 240	219.6310

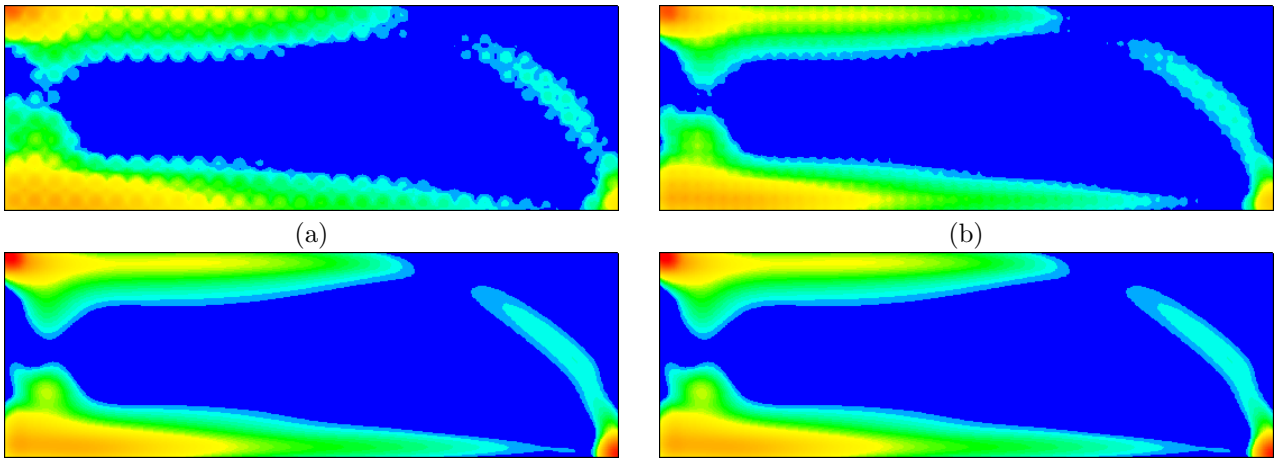

(a) (b) (c) (d)

Figure 2.8: Study of the influence of various finite element meshes on the sensitivities for a constant design variable mesh (240 x 80) (a) 30 x 10 (b) 48 x 16 (c) 240 x 80 (d) 720 x 240

Chapter 3

Pattern Gradation and Repetition

For the topology optimization formulations in Chapter 2, the concept of pattern gradation is introduced as a new constraint in the context of layout optimization. In this work (presented first in Stromberg et al. [2009]), a "pattern" is defined as the number of times a particular geometric feature repeats over a domain. Here, the ideas behind pattern repetition constraints in topology optimization designs (sometimes known as "periodic structures") are discussed with an application to the geometric stretching and shrinking of these patterns over the domain (referred to as gradation). Furthermore, a mapping scheme is proposed to map design variables from one pattern to the next throughout the domain for the element-based and CAMD approaches as presented in Chapter 2. Following, the advantages and disadvantages of each technique are briefly discussed.

The key idea behind the pattern gradation for the conceptual design of buildings presented in this work is a mapping scheme between design variables. The mapping scheme proposed in this section allows patterns of different sizes to be repeated along the height of a building to satisfy the constraints discussed in Chapter 1 for shear and overturning moments. To achieve such constraints for any set of graded patterns, the largest pattern is considered first. The design variables from the mesh over the domain that the largest pattern covers are projected onto the smaller domains using two different techniques - one for the element-based approach and a second for the CAMD. These approaches are discussed next in this section.

3.1 Element-Based Mapping Scheme

To incorporate the pattern gradation constraint, the topology optimization problem statement must be revised as follows in terms of the design variables, ρ_d and nodal displacements, $\mathbf{u}$:

$$\begin{aligned} \min_{\rho,\mathbf{u}} \quad & c(\rho_d, \mathbf{u}) \\ s.t. \quad & \mathbf{K}(\rho_d)\mathbf{u} = \mathbf{f} \\ & \int_\Omega \rho(\rho_d)\, dV \leq V_s \\ & \rho(x) \in [0,1] \,\forall\, x \in \Omega \end{aligned} \tag{3.1}$$

where the element densities and the design variables now become independent. Thus, the compliance and stiffness can be expressed in terms of the design variables ρ_d. The element densities ρ_e are a function of the design variables through a mapping scheme.

3.1.1 Gradation Along One Axis

For the element-based approach mapping in one direction, the largest domain is first saturated with design variables at the element nodes. These design variables are considered as the primary design variables (shown in grey in Figure 3.1). The primary design variables are mapped onto the smaller domains to create the mapped design variables (shown in black in Figure 3.1). Here, each pattern domain is shown by the blue colored pattern. Then, the element densities are computed using the projection method as described in Section 2.3 over the entire domain of design variables, which include both the primary and mapped design variables.

For gradation in one direction, a pattern is defined by the region of the design domain partitioned by two coordinates, denoted x_{n-1} and x_n respectively for the nth pattern. In Figure 3.1, for example, the pattern gradation is being performed in the x-direction. Thus, we specify pattern 1 by selecting the coordinates x_0 and x_1 as bounds. This concept is

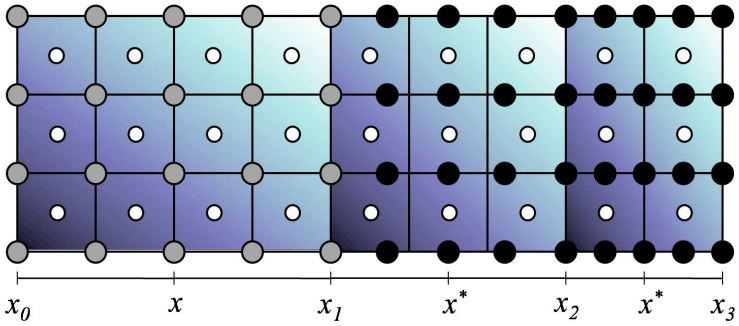

Figure 3.1: Illustration of element-based mapping scheme from x to x^* for pattern gradation along one axis. Mapped design variables are shown in black and 3 pattern constraints are highlighted in blue gradient color.

carried over for each of the n patterns.

The proposed mapping scheme for gradation in the x-direction gives the locations of the mapped design variables, x^* with respect to the pattern sizes as

$$x^* = \sum_{i=0}^{n-1}(x_{i+1} - x_i) + \alpha_n(x - x_n) \tag{3.2}$$

where α_n is a scaling factor of the nth pattern from the largest domain (which holds the primary design variables). This scaling parameter α_n is defined as:

$$\alpha_n = \frac{x_{n+1} - x_n}{x_1 - x_0} \tag{3.3}$$

Similarly, for one directional gradation along the y-axis:

$$y^* = \sum_{i=0}^{n-1}(y_{i+1} - y_i) + \beta_n(y - y_n) \tag{3.4}$$

where y^* is the location of the mapped design variable and y is the location of the original design variable. Correspondingly, the scale factor is:

$$\beta_n = \frac{y_{n+1} - y_n}{y_1 - y_0} \tag{3.5}$$

For the element-based approach, the values of mapped design variables correspond to the values of the primary design variables, $\rho^* = \rho$; only the locations of these points change

during the mapping scheme. The optimization on the design variables of the largest section is performed first and the subsequently smaller sections are updated. More details on the computational implementation are included in the following chapter.

3.1.2 Gradation Along Two or Three Axes

The mapping scheme can be extended for gradation in two directions following a two step procedure: the patterns are graded along one axis first using the largest pattern. Subsequently, these patterns are graded in the other direction using the patterns from the initial gradation. For example, if the patterns are graded along both the x and y axes, first the largest pattern is selected. This pattern is mapped along the x axis using the gradation scheme. Later, these patterns are mapped along the y axis. A schematic of this mapping procedure is shown in Figure 3.2. For the bidirectional gradation, Equations (3.2) and (3.4) still apply, but they are performed sequentially.

Furthermore, this technique can be generalized to three dimensions by the same procedure. For example, for pattern gradation along the x, y, and z axes the largest pattern is mapped sequentially in these three directions. Equations (3.2) and (3.4) still apply and an additional equation for the z-direction is introduced using a new scale factor, γ_n, as follows:

$$z^* = \sum_{i=0}^{n-1}(z_{i+1} - z_i) + \gamma_n(z - z_n) \tag{3.6}$$

where

$$\gamma_n = \frac{z_{n+1} - z_n}{z_1 - z_0} \tag{3.7}$$

3.2 Continuous Approximation of Material Distribution Mapping Scheme

The CAMD method considers a continuous material field over the design domain. Therefore, it is necessary to compute the densities for the mapped domains at the nodes to accurately

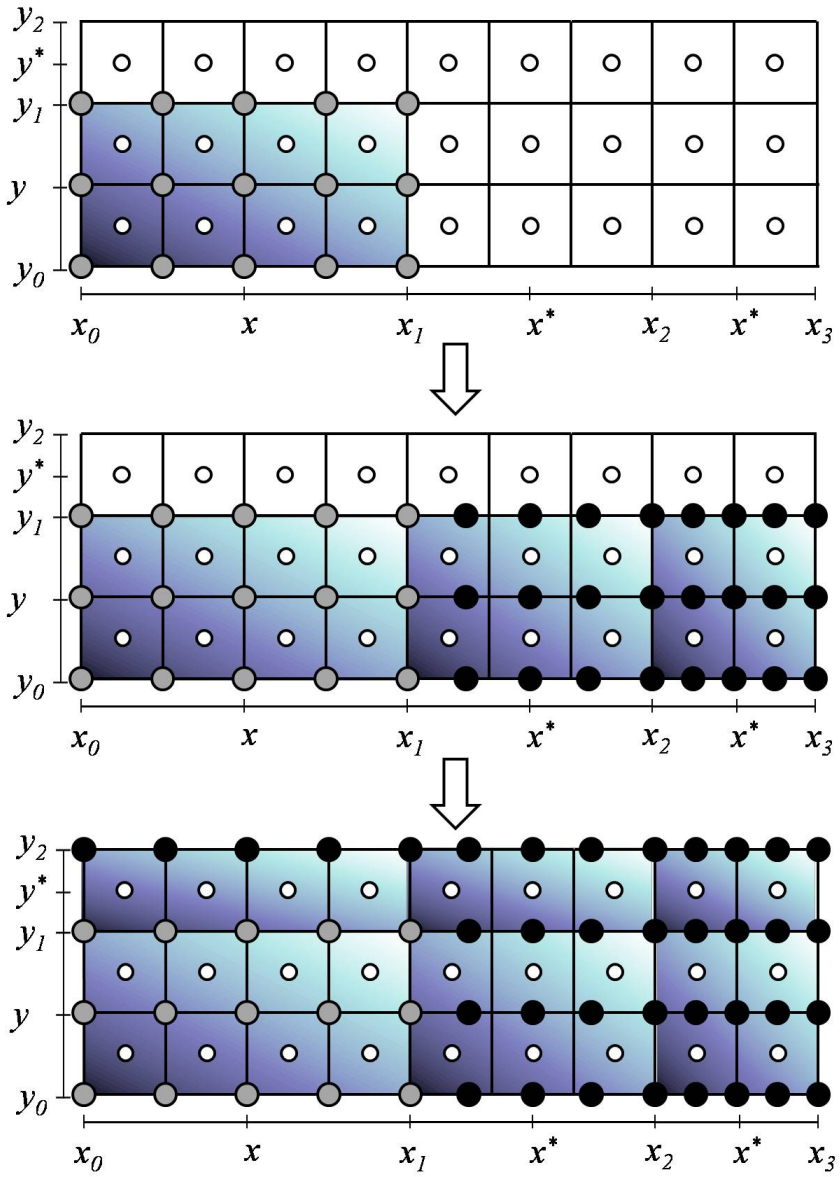

Figure 3.2: Schematic for gradation in two directions. Mapped design variables are shown in black.

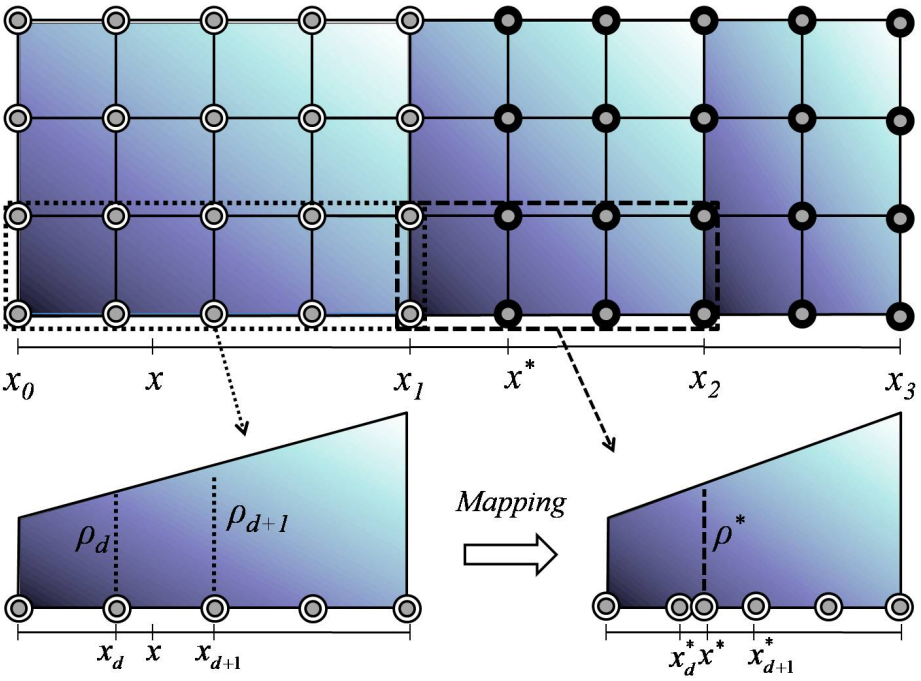

Figure 3.3: Illustration of CAMD mapping scheme: original element shown on left, interpolated design variables shown in black on right

approximate this material field. The following interpolation method is proposed to compute the nodal densities for each of the n mapped patterns. The nodes of the largest pattern are first mapped onto the domains of the smaller patterns similar to the element-based scheme described by Equations (3.2) and (3.4). The densities at the nodes of the smaller patterns are then computed by interpolating the mapped nodal densities of the largest pattern. The notation ρ_d^* and ρ_{d+1}^* is introduced for the mapped nodes closest to any node of the n patterns (see Figure 3.3). The equation for the mapped densities is

$$\rho^* = \rho_d + \frac{x^* - x_d^*}{\alpha_n}(\rho_{d+1} - \rho_d) \tag{3.8}$$

where x_d^* marks the location of the mapped design variable ρ_d in the current nth pattern, ρ^* is the new mapped density calculated at x^* and ρ_d, ρ_{d+1} are the nodes of the largest design domain to interpolate from (Figure 3.3), and α_n is still described by Equation (3.3). If α_n is replaced with β_n or γ_n and $(x^* - x_d^*)$ with $(y^* - y_d^*)$ or $(z^* - z_d^*)$ the gradation would be performed in the y-direction or z-direction instead of the x-direction. Additionally, the

gradation in two or three directions can be carried out using the same technique described in the previous section where the largest pattern is graded in one direction first and later this set of patterns is graded in the other direction via Equation (3.8). The sensitivities of the design variables need to be modified to account for the interpolation employed to compute the mapped nodal densities (see Equation 3.8). This will be described in detail in Section 3.4.

3.3 Comparison of Mapping Schemes

The pattern gradation described in the previous sections introduces additional computational expenses for the mapping scheme and sensitivity computations. However, these costs can be reduced by gathering the required data, such as the mapping information from the primary set of design variables to the mapped set of design variables for these schemes once, before the actual optimization is performed. For example, in the element-based approach at the beginning of the code the set of nodes in S_d for each of the design variables and the mapped locations of these design variables for each of the patterns are stored to easily compute the one-to-one density mapping and chain rule for the sensitivity evaluation on the fly. Likewise, in the CAMD approach for each node the information of which densities to interpolate from is stored to compute the nodal densities in a timely fashion. Then the evaluation using the updated design variables after each iteration is straightforward since only the design variables of the largest pattern need to be optimized at each iteration.

The element-based mapping scheme is easier to implement but requires storing many more design variables, especially when the ratio of the size of the largest domain to the smallest one is significantly high since there will be many design variables compacted into very small region. On the contrary, CAMD is computationally less intensive due to the smaller number of design variables. However, at the beginning of the analysis an expensive search must be performed once to find the correct primary design variables for the mapped design variables to interpolate from. Moreover, this interpolation scheme associated with

Table 3.1: Comparison of Mapping Schemes

Approach	Pros	Cons
Element-based	• no interpolation needed • one-to-one mapping of design variables • sensitivities evaluation simple using one-to-one mapping	• large number of design variables required
CAMD	• smaller number of design variables • smoother variation of density within elements	• interpolation necessary for nodal densities • initial search for nodes to interpolate from is expensive • more storage space required • sensitivity evaluation more complex

the CAMD approach is by nature more expensive than the one-to-one mapping used in the element-based approach. In conclusion, the CAMD approach, despite requiring storage of a small number of design variables, is computationally more expensive.

3.4 Sensitivities Update

The sensitivities of the design variables are computed using a chain rule since the smaller domains get their designs from the larger domains because each element density ρ_e is a function of the design variables ρ_d through the mapping schemes. Therefore, for both the element-based and CAMD approaches, the sensitivity of the objective function is now modified to include the chain rule as follows:

$$\frac{\partial c}{\partial \rho_d} = \sum \frac{\partial c}{\partial \rho_e} \frac{\partial \rho_e}{\partial \rho_d} \tag{3.9}$$

The contributions of each design variable towards the sensitivities of the primary design variables, ρ_d, are summed over each node of each element over the entire domain.

For the element-based scheme due to the one-to-one mapping, the sensitivity of each element density with respect to its primary design variable is

$$\frac{\partial \rho_e}{\partial \rho_d} = 1 \tag{3.10}$$

where e is an element that gets its density from the mapping design variable d. Equation (3.9) can now be simplified as

$$\frac{\partial c}{\partial \rho_d} = \sum_{e \in S_d} \frac{\partial c}{\partial \rho_e} \tag{3.11}$$

where S_d denotes the subset of design variables sharing the same density. For example, if there are n patterns present, S_d contains n values.

In the CAMD mapping scheme, the sensitivities of each node must include the contributions from the nodes that are interpolated from ρ_d and ρ_{d+1}. Thus, for each mapped element e the following two relationships ensue:

$$\frac{\partial \rho_e}{\partial \rho_d} = 1 - \frac{x^* - x_d^*}{\alpha_n} \tag{3.12}$$

and

$$\frac{\partial \rho_e}{\partial \rho_{d+1}} = \frac{x^* - x_d^*}{\alpha_n} \tag{3.13}$$

In these equations α_n describes the gradation in the x-direction. The gradation in the y-direction or z-direction is similarly derived. For gradation along two or three axes, the sensitivities are the same, but they must be computed sequentially.

3.5 Projection Update

For the previously discussed approaches, the design domains for each repetition of a graded pattern are scaled from the largest pattern. Thus the projection weighting function must be reformulated over the graded patterns. In this work, a new projection scheme is proposed by changing the domain of influence for element e to be elliptical in shape to satisfy the gradation constraint. This can be attributed to the fact that the mapped distances between design variables are scaled by the factor α_n or β_n. The ellipse has a major axis of $2r_{min}$ and a minor axis of $2\alpha_n r_{min}$ corresponding to a circle scaled in one direction (see Figure 3.4(c)). Some difficulties arise when this domain of influence lies over a boundary of the patterns. Thus, a hybrid between a circular region and an elliptical region is proposed for

the projection scheme (see 3.4(b)). The weights are now computed as

$$w_j^e = \begin{cases} \left(\frac{r_{min} - r_j^e}{r_{min}}\right)^q & r \leq r_{min} \\ 0 & r > r_{min} \end{cases} \tag{3.14}$$

where r_j^e is described by

$$r_j^e = \begin{cases} x_j - x_e & x_j \epsilon \Omega_e,\ x_0 \leq x_j \leq x_1,\ x_0 \leq x_e \leq x_1 \\ \frac{(x_j - x_1)}{\alpha_n} + (x_1 - x_e) & x_j \epsilon \Omega_e,\ x_1 < x_j,\ x_0 \leq x_e \leq x_1 \\ \frac{(x_e - x_1)}{\alpha_n} + (x_1 - x_j) & x_j \epsilon \Omega_e,\ x_1 < x_e,\ x_0 \leq x_j \leq x_1 \\ \frac{(x_j - x_e)}{\alpha_n} & x_j \epsilon \Omega_e,\ x_1 < x_j,\ x_1 < x_e \\ 0 & otherwise \end{cases} \tag{3.15}$$

These modifications allow the design to be continuous throughout the domain while still enforcing the pattern constraints. With the revised weights above, the domain, Ω_e, over which the projection is computed remains in theory the same as a domain with no gradation in which the largest pattern is repeated n times.

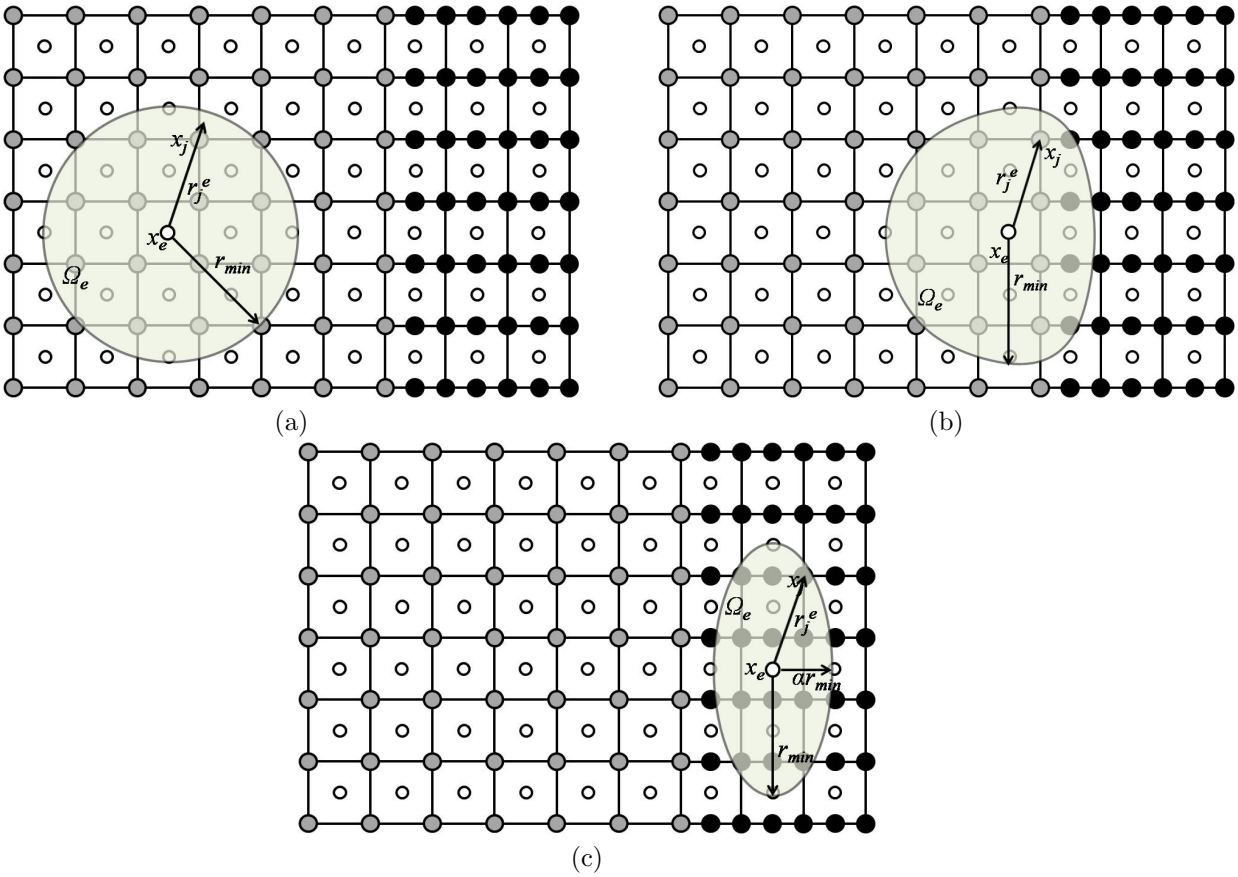

Figure 3.4: Examples of three different projection domains for pattern gradation: (a) circular, (b) hybrid, and (c) elliptical. The design variables are shown in white; these design variables are mapped in black for the graded pattern.

Chapter 4

Computational Implementation

The computational implementation of the theory discussed in Chapters 2 and 3 is described in this chapter. The computations were carried out using Matlab®. The visualization of the results was done using Matlab® primarily for 2D problems and Tecplot® for the 3D problems. The specifics behind the Matlab coding are discussed next.

Both the CAMD and the element-based approaches are implemented as mentioned in the previous chapter; however, the two methods differ in some aspects. For example, in the pattern gradation mapping function, the CAMD code gathers first the information needed for the interpolation between nodes. Then, in the integration of the stiffness matrix, the densities of the material at each Gauss point must be used. On the other side, the element-based approach consists of a uniform density throughout the element so the density for the element can be used.

4.1 Implementation Issues

The flowchart in Figure 4.1 outlines the general ideas behind the code, which is designed to guarantee robustness. The first step is reading a mesh. In this work, the mesh is generated either using a mesher written in Matlab® or using the PATRAN® software package. After generation, the mesh is refined to a very fine level for the MTOP implementation. The original mesh passed to the program is used as the displacement mesh in the finite element analysis. The necessary data is then gathered for the manufacturing constraints mapping, which includes pattern gradation and symmetry. Depending on the approach used in the solution (i.e. element-based or CAMD) the information collected varies. For the element-

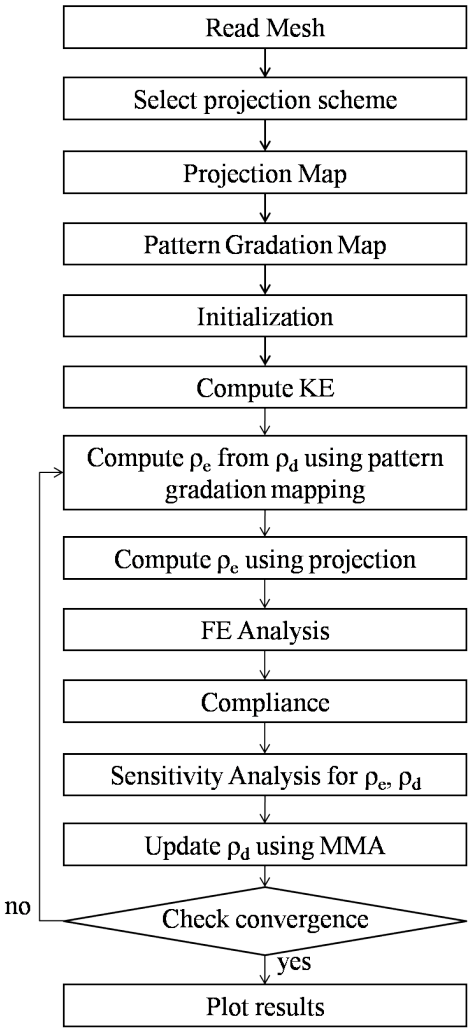

Figure 4.1: Flowchart of Computer Code for Pattern Gradation

based approach, the locations of the new design variables are required. Such locations simply coincide with the nodes of the mesh for the CAMD approach. Moreover, the CAMD approach must store the necessary information for the interpolation of the primary design variables in the optimization. After all the required information is collected for both approaches, a search is performed over the design domain to gather information for the projection using a fixed-length scale. Specifically, the weights for each density element are computed and stored for use throughout the iterations. There is an option for the user to select which projection scheme to use (direct or inverse) along with which curve (linear, parabolic, cubic, etc.)

The optimization process begins with a simple initialization of all of the design variables and densities uniformly over the domain to the specified volume fraction. Here we also set the minimum values for the intermediate densities, $\rho_{min} = 0.001$ to prevent the singularity of the stiffness matrix discussed earlier. Next, the element stiffness matrix can be computed once at the beginning (if all elements are of the same size).

After these initial steps, the loop for the actual optimization begins where first the element densities are computed using the updated design variables from the pattern gradation mapping. Then, the element densities can be updated using the weights computed in the projection map. Now, these updated densities are given to the finite element analysis function, which computes the global stiffness matrix and updates the forces accordingly. Then Cholesky decomposition is applied to solve the system of equations. The resulting displacements are used to then compute the compliance and corresponding sensitivities which are finally given to the MMA solver (see Svanberg [1987]) for the update. Convergence criteria is checked and the code terminates if it is satisfied. Finally, the solution is plotted using Matlab® or Tecplot®.

The pseudo-code for the 2D element-based implementation is provided in the Appendix.

4.2 Discussion

The search to gather the required information for the projection method implemented has a very high computational cost. To alleviate some of these costs, the domain of design variables can be partitioned into sections of size r_{min} by r_{min}. Then, for each element, only the neighboring sections need to be searched, rather than the entire design domain. The mapping function for the pattern gradation implementation poses an additional computational expense as well. A similar approach to that of finding the weights for the projection can be used at the beginning of the code so that this routine must complete only once, reducing this expense.

One last point to mention is that all of the coding presented here uses constraints based on the model's geometry rather than the input mesh. For example, pattern sizes and radius of projection are specified in terms of geometrical coordinates instead of number of elements. This provides for a more general coding since upon refinement of a mesh, it is unnecessary to scale the parameters accordingly.

Chapter 5

Numerical Results

Several examples with various numbers and sizes of patterns are solved for the pattern gradation implementation presented in this work. In this chapter, two-dimensional examples are given including cantilever beams subject to lateral loads while the three-dimensional examples given explore building-like domains subject to wind loadings. All examples are run using SIMP with continuation from $p = 1$ to 4 with steps of size 0.5. The Poisson's ratio is 0.3 and Young's Modulus, $E = 1.0$. Examples are given next for both the element-based and CAMD approaches.

5.1 Domain with Two Patterns

Using the element-based approach with the design variables placed at the nodes, the cantilever beam problem in Figure 5.1 is solved with the modified projection scheme as described in Section 3.5. The primary and mapped design variables are shown in Fig. 5.1(b) in blue and red respectively. The domain is 10 x 30 units with the fine mesh containing 80 x 240 elements. The volume fraction for this example is 0.5 and the minimum member size is 1.2 units. The patterns shown have a ratio of 2:1.

5.2 Domain with Five Patterns

Next, an example is given for a two-dimensional building-like problem subject to a lateral wind loading and pattern constraints as displayed in Figure 5.2(a). The domain is 10 x 30 units with the fine mesh containing 80 x 240 elements. The volume fraction for this example

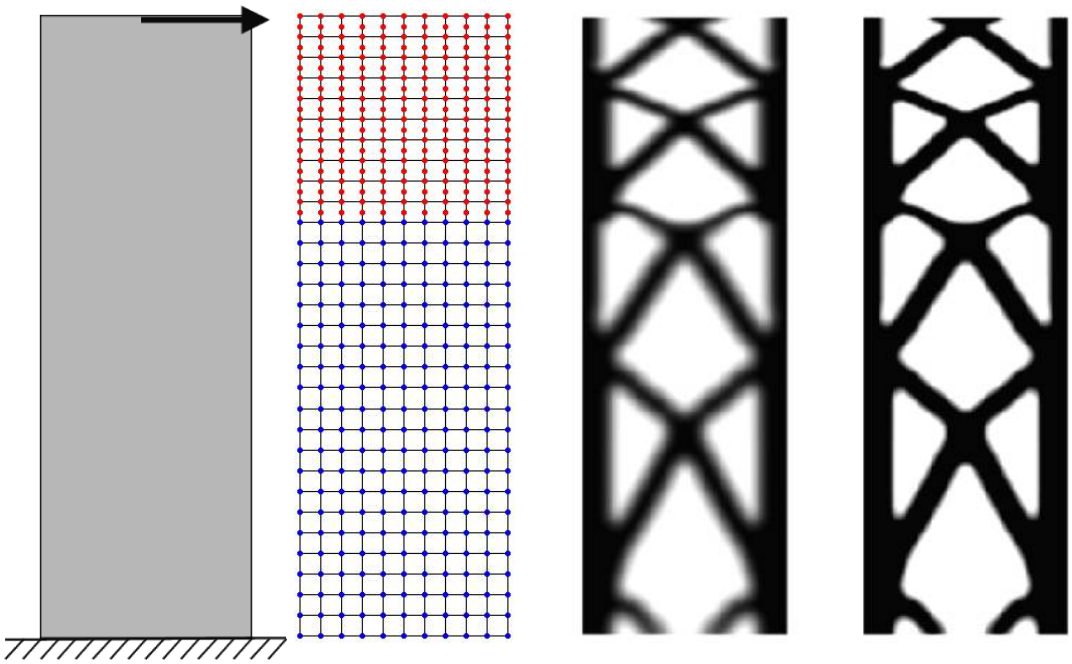

Figure 5.1: Element-based approach for pattern gradation in a cantilever beam with 2 patterns: (a) problem statement, (b) design variable mesh, (c) topology optimization solution and (d) proposed design. Mapped design variables are shown in red.

is 0.5 and the minimum member size is 1.2 units. As shown in the figure, some similarities can be observed in comparison with the lateral bracing system of the John Hancock building in Chicago, IL.

5.3 Bidirectional Gradation for Deep Beam

The effect of grading the patterns along two axes is given in Figure 5.3 for a deep cantilever beam supported along the left edge with a point load at the lower right tip. The element formulation for this example is the continuous approximation of material distribution with an interpolation scheme described in Sections (2.2.2) and (3.1.2). The result given is for a mesh size of 40 x 20, with the MTOP fine mesh of 200 x 100 (Q4/n25 elements). This example was run with continuation from $p = 1$ to 4 with steps of size 0.5.

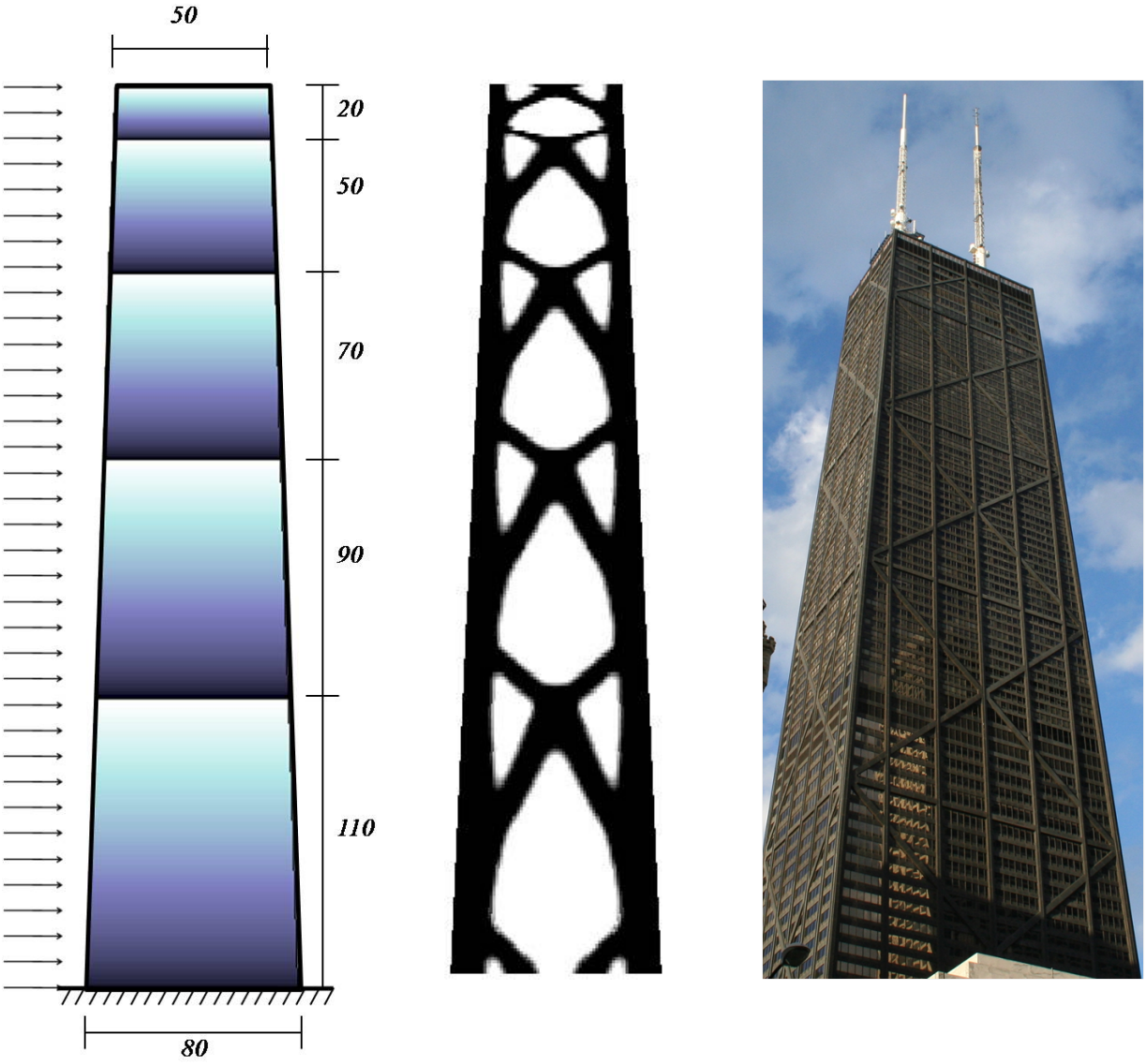

(a) (b) (c)

Figure 5.2: Illustration of the concept of pattern gradation along the height of a building (similar to the John Hancock building in Chicago, IL)

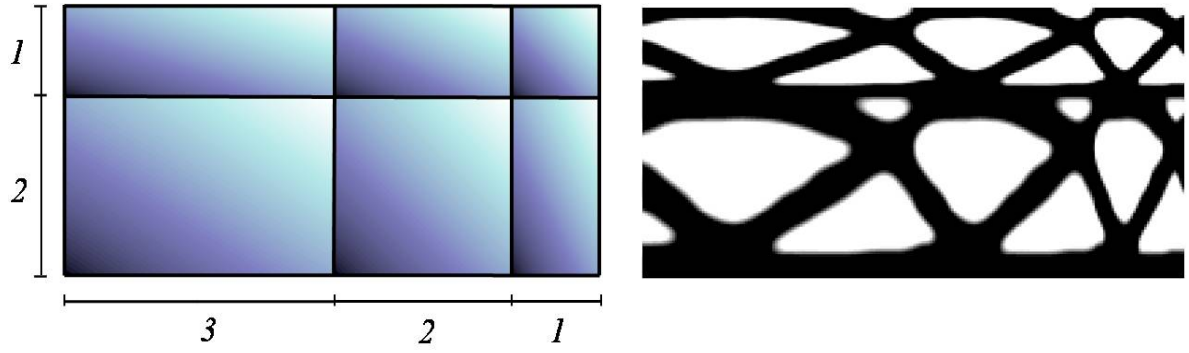

(a) (b)

Figure 5.3: Example of pattern gradation along both x and y axes using CAMD mapping scheme: (a) pattern gradation constraints (in blue) (b) topology optimization result

5.4 Torsional Building with Four Patterns

Figure 5.4 is an example of a building subject to a torsion load. The finite element mesh is 10x10x30 with the same pattern constraints as the 2D example given in Figure 5.2. The result here was run using SIMP with $p = 3$. Figure 5.4(a) and (b) show the solution with MTOP B8/n8 elements, while Figure 5.4(c) and (d) show the results for MTOP B8/n27 elements.

5.5 Building Core

Figure 5.5 illustrates a conceptual design for a building core system to support the cantilevered slabs shown in (a). This structure is subject to pattern gradation constraints of 15, 12, 10, 8, 7, 5 and 3 from bottom to top to achieve a desirable transition from a large bracing angle at the base of the structure to resist the overturning moment due to wind loads and a shallow angle at the top to resist the large shear loads. The design domain is 10 x 10 x 50 here with 16,000 elements and a minimum member size of 1.0.

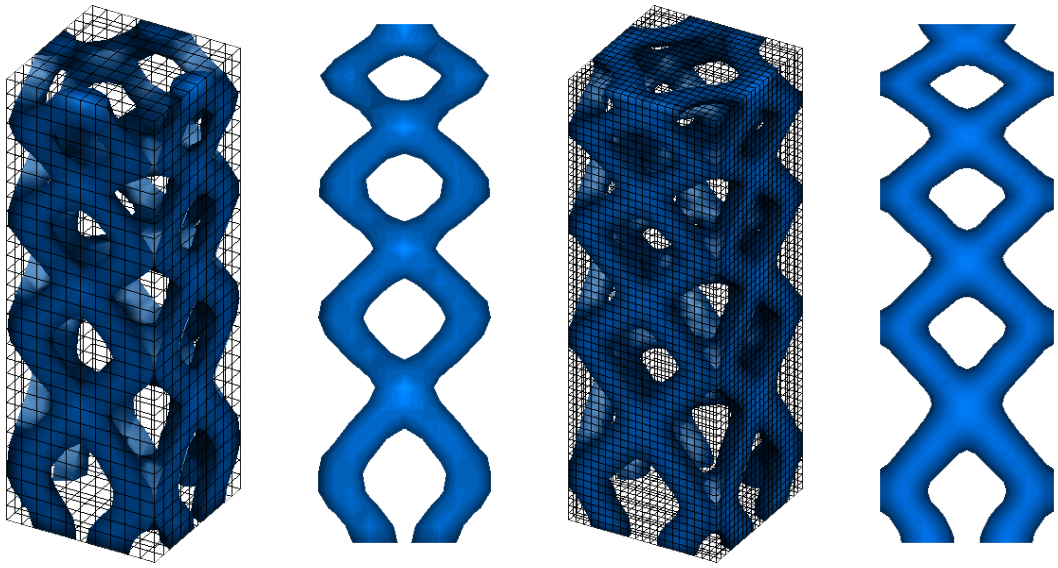

(a) (b)

Figure 5.4: Illustration of pattern gradation for conceptual design of building subject to torsional load (a) for 10x10x30 mesh (b) and 10x10x30 with MTOP Q4/b8 elements

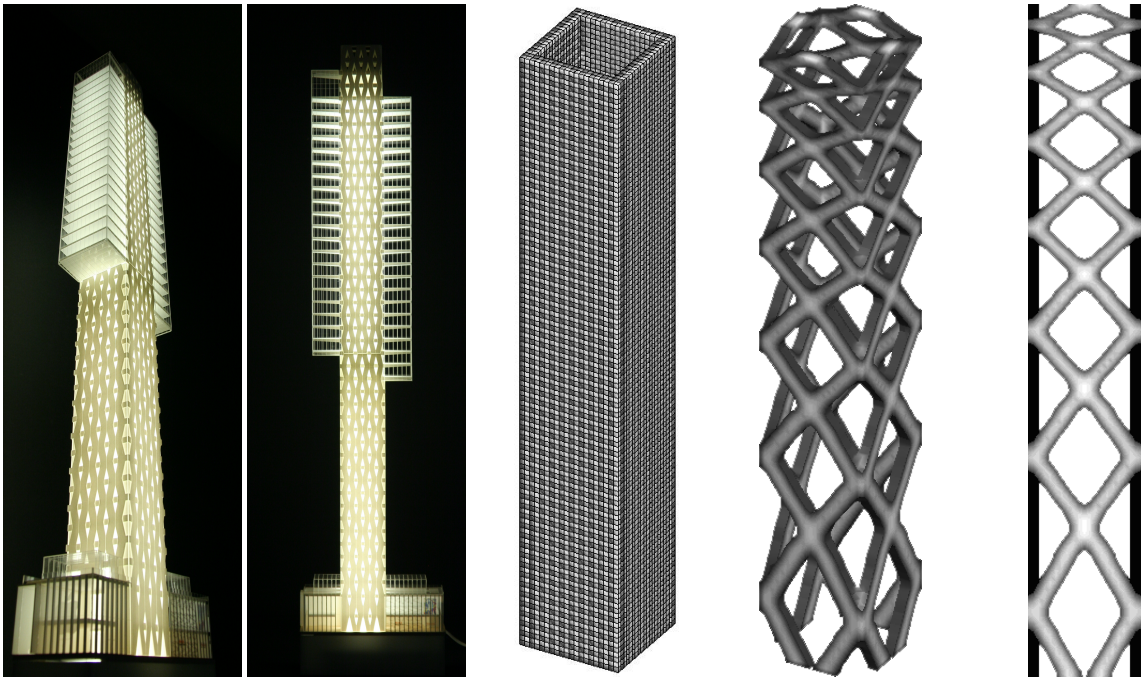

(a) (b) (c) (d) (e)

Figure 5.5: Illustration of pattern gradation for conceptual design of building core. (a),(b) Design domain, (c) FEM Mesh (20 x 20 x 120), (d),(e) Proposed core design using pattern gradation. Images (a) and (b) courtesy of Skidmore, Owings & Merrill, LLP (SOM)

5.6 Diagrid Structure with Wind Loading

Figures 5.6, 5.7 and 5.8 illustrate a conceptual design for a diagrid structure with a square base transitioning to a circle around the top. The meshing of this structure is illustrated in Figure 5.6 where the cross-sectional views are shown along the height of the tower at 0, 30, 60, and 80m. In Figure 5.7 the results are shown for an analysis performed for a wind loading in one direction with symmetry and wind loads with symmetry applied about the center in two directions.

To emphasize the patterns of the geometry, Figure 5.8 shows the natural pattern that develops along the shear lines in addition to an analysis performed with pattern gradation constraints. The design domain is 10 x 10 x 80 here with a minimum member size of 1.0. Notice the resulting designs follow the principal stress trajectories, the columns increase in size from the top of the building to the base, the diagonals intersect at 45 degrees along the neutral axis with larger angles at the base than the top, and the load flows in a naturally cascading pattern.

5.7 Discussion and Limitations

The work presented in this section would benefit tremendously from the use of a more advanced data structure (see Celes et al. [2005]) since it can be quite complex to use the multiresolution scheme (MTOP) for general meshes. Currently, the connectivity relationships between the coarse mesh of displacements and the fine meshes of design variables or densities are unknown. A more elaborate scheme using multiple meshes should be considered to advance this work further for general meshes.

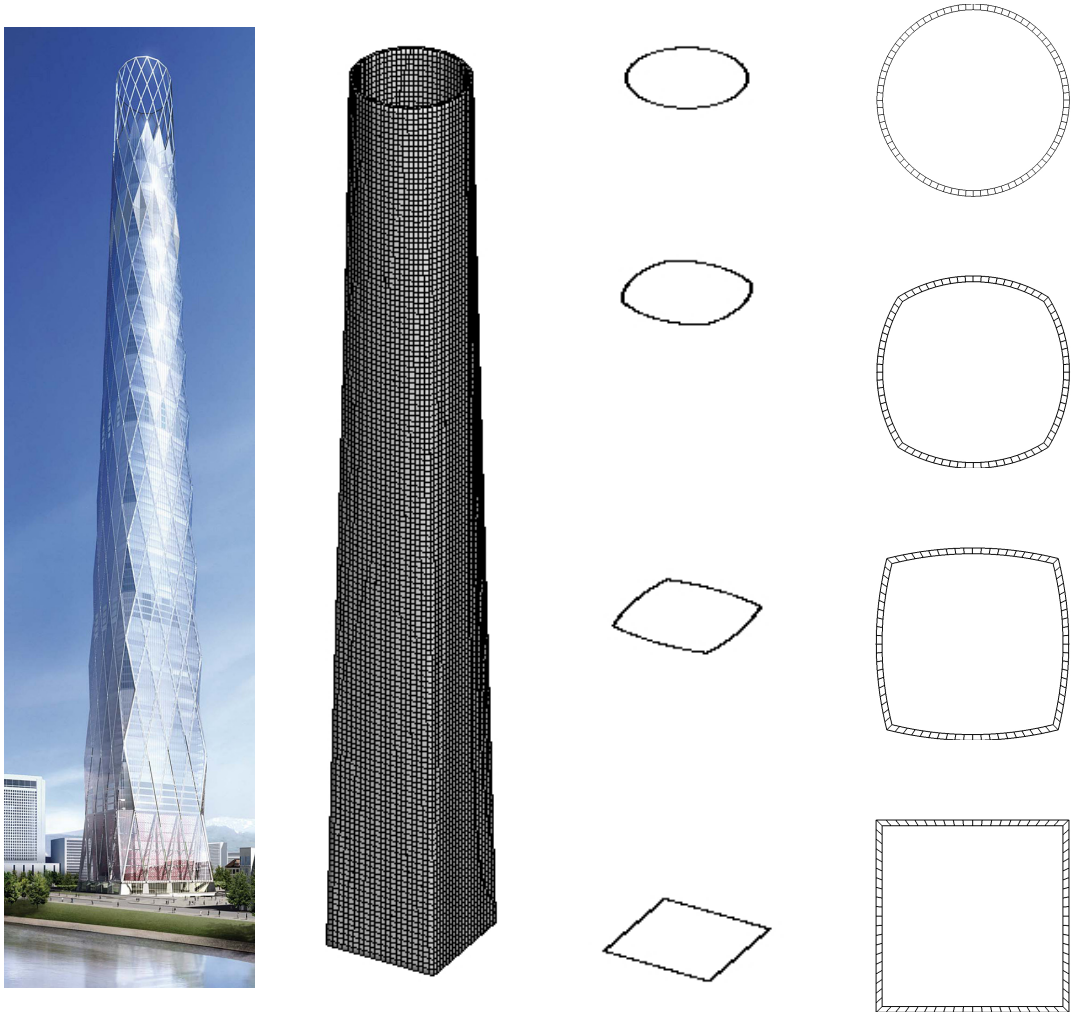

(a) (b) (c) (d)

Figure 5.6: Illustration of meshing for diagrid structure: (a) SOM's Lotte Tower, (b) Finite element mesh, (c),(d) Cross-section views at 0, 30, 60, and 80m. Image (a) courtesy of Skidmore, Owings & Merrill, LLP (SOM)

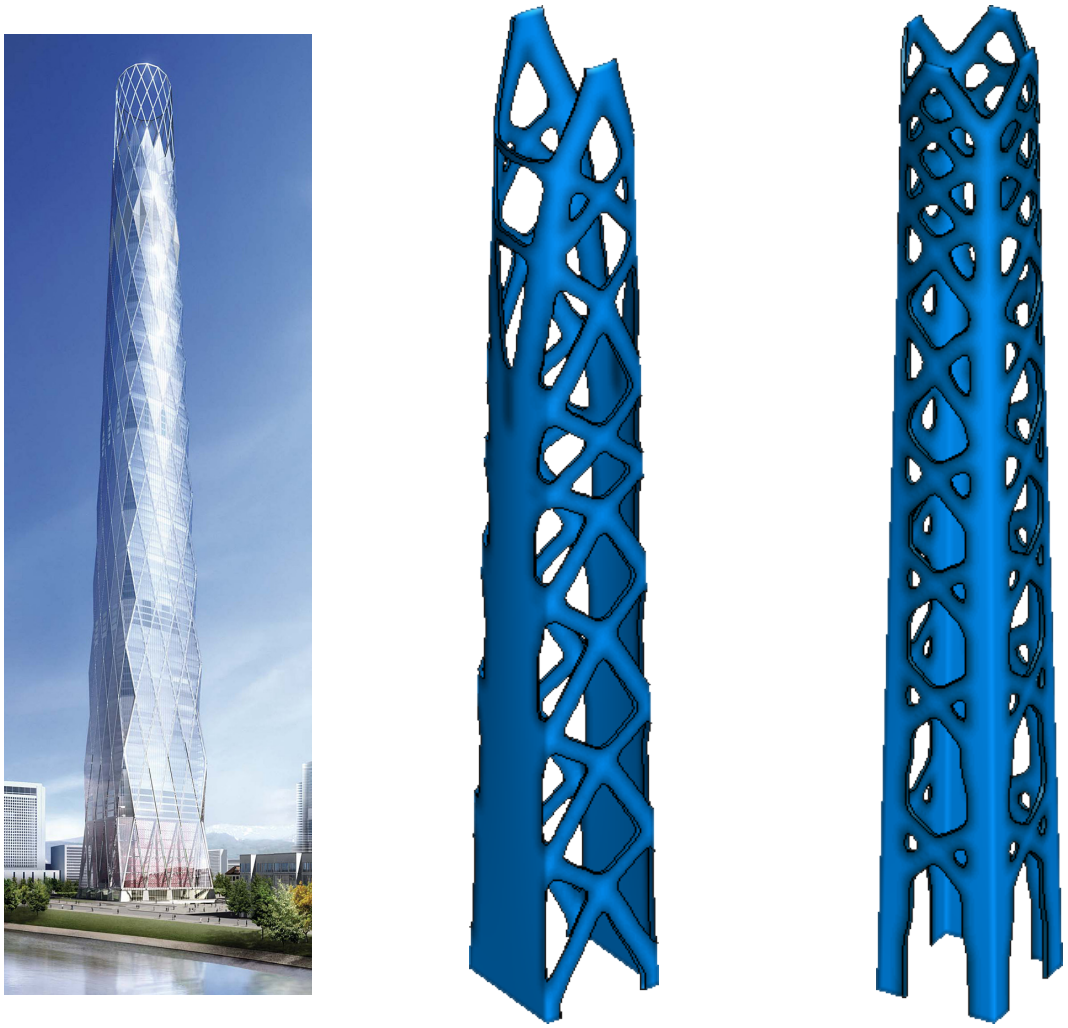

(a) (b) (c)

Figure 5.7: Illustration of pattern gradation for conceptual design of diagrid structure: (a) SOM's Lotte Tower, (b) Wind loading about 1 axis and symmetry, (c) Wind loading about 2 axes and symmetry. Image (a) courtesy of Skidmore, Owings & Merrill, LLP (SOM)

(a) (b) (c)

Figure 5.8: Illustration of pattern gradation for conceptual design of diagrid structure: (a) SOM's Lotte Tower, (b) Torsion loading without constraints, (c) Pattern gradation constraints. Image (a) courtesy of Skidmore, Owings & Merrill, LLP (SOM)

Chapter 6

Concluding Remarks and Extensions

Pattern gradation is necessary to advance topology optimization towards more practical designs for constructibility of high-rise buildings. By adding constraints on the patterns, both engineers and architects are able to develop aesthetically appealing modern designs while satisfying structural requirements. Moreover, using the techniques presented in this work, structural engineers can design the diagrid-type lateral bracing systems of buildings by identifying along the height of the building the optimal angles for the diagonal members therefore allowing a smooth transition between the sharp angle at the base to resist overturning moments and the shallow angle at the top to account for shear loads.

The primary contributions of this work can be briefly summarized as follows:

- Conceptual design for buildings by placing constraints on the design domain in terms of number and size of repeating patterns along any direction
- Development of mappings to geometrically grade the patterns
- Incorporation of projection techniques in conjunction with the mappings (use of elliptical rather than circular domains of influence)

6.1 Suggestions for Future Work

While the work presented here is sufficient for smaller-scale designs, it would benefit tremendously by exploring in more detail the computational expenses associated with non-coincident FEM displacement and design variable meshes to be used on a larger scale. Moreover, by studying the sensitivities associated with non-coincident meshes, a basis could be established

for error estimators. Future work includes the optimization of large scale problems using Topological Data Structure (TopS) [Celes et al., 2005] integrated with finite element analysis (TopFEM) and topology optimization.

Furthermore, some additional building design considerations to investigate in more detail include the sizing of members from topology optimization results in addition to other objective functions or constraints which might include deflection considerations, stress constraints and stability issues. The work here would also benefit from studying the nonlinear behavior associated with large deflections for high-rise buildings and other structures. A few other extensions of this work including the modeling of subdomains, extension to other types of finite elements, and the integration with commercial software are described in more detail next.

Modeling of Subdomains

Within the context of building design, it might be useful for the designer to look a component of a structural system, such as a deep transfer beam. The present work could be extended to model subdomains of the structural system using static decomposition where the loads and designs of connecting members or adjacent subdomains are replaced with boundary conditions.

Extension to Other Finite Elements

Though Q4 and B8 elements were sufficient for the examples given in this work, topology optimization for buildings could become more robust by including other types of finite elements such as beams, plates and shells. The use of Q4 or B8 elements are not as robust as plates, shells, or beams because each of these finite elements have explicit terms (shape functions) for the moment and shear components, while the Q4 or B8 only has nodal forces. These moment and shear components are advantageous to have since they make these elements more compatible with the current design codes. Moreover, an analysis using higher-order elements could be performed efficiently using an application programming interface (API)

to call an FEM software, such as ABAQUS® or ANSYS® and then integrating the results with the optimization process.

Integration with Commercial Software

Finally, a continuation of this work is to explore a more interactive framework between the structural engineering presented here and the architectural parameters both technical (need for stairs, elevators, mechanical openings, etc.) and aesthetic (design value of the structure). More specifically, this work would benefit the structural engineering industry by extending its capabilities to integrate with architectural software, especially exporting the geometry of results to AutoCAD® or others. Additionally, a user friendly interface with input parameters could be created to incorporate structural engineering, aesthetics and topology optimization for use in today's design companies.

Multiscale Topology Optimization

To understand the behavior of an entire structural system, it is crucial to consider all of its features at multiple scales. For example on the global scale, there is the design of the lateral system (diagonal bracing or core) to be optimized. At the local scale, there are the individual beams and columns which comprise the structural system. The way the global and local loads are transferred and how each scale interacts must be carefully analyzed to perform topology optimization for an *entire* structural system.

Appendix A

Pseudo-Code for Pattern Gradation in Topology Optimization

```
================================================================================
   Pseudo-Code for main function
================================================================================
 Inputs:

 element: a cell structure containing each node in cell i,1 for element i
 node: the locations of each node i stored as nodes(i,:) = [x, y]
 supp: the list of supports as supp(i,:) = [node, constraint x, constraint y] where
 constraint is 0(free) or 1(fixed)
 load: the list of loads as [node, force x, force y]
 element MTOP: the connectivity of the underlying fine mesh to be used for the design
 variable and density meshes for the MTOP implementation
 node MTOP: the nodal locations corresponding to the MTOP elements
 rmin: the radius of projection
 p: the penalization factor for SIMP
 rfnmt: the amount each direction is refined for MTOP implementation
 volfrac: the volume fraction constraint

 Selected function variables:

 xe: element
 xd: design variables for entire domain
 xmc: primary design variables for pattern
 c: compliance
 dc: sensitivities of the compliance
 KE: element stiffness matrix
 Ue: element displacements
================================================================================

 CALL sub-function (mc map) with (element,node) to compute (mc vals)
 CALL sub-function (proj map) with (element,node,rmin) to compute (weights)
 xe <- volfrac; xd <- volfrac; xmc <- volfrac;
 c <- 0; dc <- 0; xmin <- 0.001;
 CALL sub-function (lk) to compute (KE)

 << Loop for optimization >>
 FOR all values of penalization DO
    FOR all loops until max iter DO
       CALL sub-function (proj_densities) with (weights,xe) to compute (xe)
       CALL sub-function (mc_dvs) with (mc_vals,x_mc) to compute (xd)

       << FE Analysis >>
       CALL sub-function (FE) with (element,element MTOP,node,node MTOP,supp,load,xe,p,KE,rfnmt)
       to compute (U)
```

```
      << Objective function and sensitivity analysis >>
      CALL (sens) with (element,element MTOP,node,node MTOP,U) to compute (c,dc)

      << Update design variables using Svanberg's MMA sub-routine >>
      CALL (mmasub) with (constraint,c,xold1,xold2,dc,dv) to compute (xmma)
      xold2 <- xold1; xold1 <- xd; xd <- xmma;

      << Check convergence >>
      IF change < 0.01 THEN
         break;
      END IF
      Print (loop,c,volume,change)
   END FOR
END FOR
Plot converged solution

=============================================================================
  Pseudo-code for mc_map sub-function
=============================================================================
Inputs:

element: a cell structure containing each node in cell i,1 for element i
node: the locations of each node i stored as nodes(i,:) = [x, y]

Outputs:

mc_vals: mapping values for primary design variables to secondary design variables
centroids: centroids of each element
area: vector of areas of each element
proj_dvs: locations of all primary and secondary design variables
=============================================================================

User prompt for x min, x max, y min, y max of primary design domain
FOR all elements DO
   Compute the centroid and area of each element using polyarea
END FOR

<< Get domain of primary design variables >>
FOR all elements DO
   Search for design variables in [x min,x max]&[y min,y max]
   mc_vals{dv,1} <- primary design variable
END FOR
FOR each pattern DO
   FOR each design variable DO
      new_dv project primary design variable onto smaller domain
      mc_vals{dv,1} <- [mc vals{dv,1}, new dv]
      proj_dvs <- location of new projected design variable
   END FOR
END FOR

=============================================================================
  Pseudo-code for proj_map sub-function
=============================================================================
Inputs:

element: a cell structure containing each node in cell i,1 for element i
node: the locations of each node i stored as nodes(i,:) = [x, y]
rmin: minimum radius of projection
```

```
Outputs:

weights: list of projection weights
================================================================================

 prompt user for projection scheme (linear, inverse, parabolic, etc.)
 << Search for design variables within projection radius >>
 FOR each density DO
    x <- x coordinate of element centroid;
    y <- y coordinate of element centroid;
    z <- z coordinate of element centroid;
    FOR each design variable DO
       r <- sqrt((x+xi)^2+(y+yi)^2)
       IF r < rmin THEN
          compute and store weights using appropriate scheme
       END IF
    END FOR
 END FOR

 << Normalize weights for each density >>
 FOR each density DO
    weights <- weights/sum(weights{element})
 END FOR

================================================================================
   Pseudo-code for proj_densities sub-function
================================================================================
 Inputs:

 x_old: current element (or nodal) densities
 weights: computed weights from projection mapping

 Output:

 x_new: updated densities
================================================================================

 FOR all elements in domain DO
    x_new <- (weights{element}*x_old(elements))/sum(weights{element})
 END FOR

================================================================================
   Pseudo-code for mc_dvs sub-function
================================================================================
 Inputs:

 x primary: the primary design variables
 mc_vals: the mapping values

 Output:

 x_mapped: the values of the secondary or mapped design variables
================================================================================

 FOR all design variables in the domain DO
    FOR each primary design variable DO
       x_mapped <- x_primary using mc_vals
```

```
   END FOR
END FOR

================================================================================
  Pseudo-code for FE sub-function
================================================================================
Inputs:

element: a cell structure containing each node in cell i,1 for element i
node: the locations of each node i stored as nodes(i,:) = [x, y]
supp: the list of supports as supp(i,:) = [node, constraint x, constraint y] where
constraint is 0(free) or 1(fixed)
load: the list of loads as [node, force x, force y]
element MTOP: the connectivity of the underlying fine mesh to be used for the design
variable and density meshes for the MTOP implementation
node MTOP: the nodal locations corresponding to the MTOP elements
rmin: the radius of projection
p: the penalization factor for SIMP
rfnmt: the amount each direction is refined for MTOP implementation
volfrac: the volume fraction constraint
element MTOP
node MTOP
xe: element densities from previous iteration
KE: element stiffness matrix

Outputs:

U: vector of displacements for each node

Select function variables:

K: global stiffness matrix
edof: element degrees of freedom
fixed_dofs: prescribed degrees of freedom (from supp)
free_dofs: degrees of freedom
all_dofs: the union of fixed dofs and free dofs
================================================================================

CALL sub-function (lk) to compute (KE) if not done previously
K <- 0; f <- 0;
FOR all elements in the domain DO
   get degrees of freedom for each element
   assemble global stiffness matrix using dofs
END FOR

<< Define loads and supports >>
nload <- size of load
f(load(1:nload,1)) <- load(1:nload,2)
f(load(1:nload,1)+nnode) <- load(1:nload,3)
fixed_dofs <- prescribed dofs
all_dofs <- 1:2*nnode
free_dofs = all_dofs - fixed_dofs

<< Solve for nodal displacements >>
Solve linear system using K(free dofs,free dofs),f(free dofs) for U(free dofs)
U(fixed_dofs) <- 0

================================================================================
```

```
  Pseudo-code for lk sub-function
================================================================================
 Inputs:

 node: the locations of each node i stored as nodes(i,:) = [x, y]
 enode: list of nodes corresponding to the element

 Outputs:

 K: global stiffness matrix

 Selected local variables:

 B: strain-displacement matrix
 C: plane-stress constitutive matrix
 J0: Jacobian matrix relating natural to physical coordinates
================================================================================

 E = 1; nu = 0.3;
 C = E/(1-nu^2)*[1 nu 0; nu 1 0; 0 0 (1-nu)/2];
 Q <- locations of Gauss Quadrature points
 W<-weights of Gauss Quadrature points
 FOR each quadrature point DO
    CALL (shapequad) sub-routine to compute (N,dNdx) using (Q,W)
    compute Jacobian
    assemble B using dNdx
    K <- KE + B'*C*B*W*det(J0)
 END
================================================================================
  Pseudo-code for shapequad sub-function
================================================================================
 Input:

 x: x-coordinate of location to compute N, dNdx
 y: y-coordinate of location to compute N, dNdx

 Outputs:

 N: evaluation of shape functions at point (x,y)
 dNdxi: evaluation of shape function derivatives at point (x,y)
================================================================================

 N = 1/4[(1-x)*(1-y);(1+x)*(1-y);(1+x)*(1+y);(1-x)*(1+y)]

 dNdxi = 1/4[-(1-y) (1-y) (1+y) -(1+y); -(1-x) -(1+x) (1+x) (1-x)]

================================================================================
  Pseudo-code for sens sub-function
================================================================================
 Inputs:

 element: a cell structure containing each node in cell i,1 for element i
 node: the locations of each node i stored as nodes(i,:) = [x, y]
 U: nodal displacements
 weights: weights computed in proj map

 Outputs:
```

```
 c: compliance (objective function)
 dc_d: sensitivities of the objective function with respect to projection and then
 manufacturing constraints
================================================================================

 c <- 0;
 FOR all elements DO
    get edofs
    calculate c using U(edofs)
    calculate dc
 END FOR

 << Calculate sensitivities using projection >>
 FOR all elements DO
    compute dc_x using (dc,weights)
 END FOR

 << Calculate sensitivities using manufacturing constraints >>
 FOR all design variables DO
    FOR each primary design variable DO
       compute dc_d using dc_x
    END FOR
 END FOR

================================================================================
```

References

S. R. N. Almeida, G. H. Paulino, and E. C. N. Silva. A simple and effective inverse projection scheme for void distribution control in topology optimization. *Structural and Multidisciplinary Optimization*, 39(4):359–371, 2009.

S. R. N. Almeida, G. H. Paulino, and E. C. N. Silva. Material gradation and layout in topology optimization of functionally graded structures: a global-local approach. *Structural and Multidisciplinary Optimization*, 2010. Accepted for publication.

L. Ambrosio and G. Buttazzo. An optimal design problem using perimeter penalization. *Calculus of Variations and Partial Differential Equations*, 1(1):55–69, 1993.

AISC Steel Construction Manual, Thirteenth Edition. American Institute of Steel Construction, Inc., 2005.

M. P. Bendsoe. Optimal shape design as a material distribution problem. *Structural Optimization*, 1(4):193–202, 1989.

M. P. Bendsoe and O. Sigmund. Material interpolation schemes in topology optimization. *Archive of Applied Mechanics*, 69(9–10):635–654, 1999.

M. P. Bendsoe and O. Sigmund. *Topology optimization: theory, methods and application*. Springer, New York, 2003.

T. Borrvall and J. Petersson. Topology optimization using regularized intermediate density control. *Computer Methods in Applied Mechanics and Engineering*, 190(37-38):4911–4928, 2001.

B. Bourdin. Filters in topology optimization. *International Journal for Numerical Methods in Engineering*, 50(9):2143–2158, 2001.

J. Cagan, K. Shimada, and S. Yin. A survey of computational approaches to three-dimensional layout problems. *Computer-Aided Design*, 34:597–611, 2002.

R. C. Carbonari and G. H. Paulino. Multi-actuated functionally graded piezoelectric microtools design: A multiphysics topology optimization approach. *International Journal for Numerical Methods in Engineering*, 77(3), 2009.

W. Celes, G. H. Paulino, and R. Espinha. A compact adjacency-based topological data structure for finite element mesh representation. *International Journal for Numerical Methods in Engineering*, 64(11):1529–1556, 2005.

A. R. Diaz and O. Sigmund. Checkerboard patterns in layout optimization. *Structural Optimization*, 10(1):40–45, 1995.

K. Gerfen. 2009 R+D Awards: Oasis Generator. *Architect*, pages 54–55, August 2009.

J. K. Guest. Imposing maximum length scale in topology optimization. *Structural and Multidisciplinary Optimization*, 37(5):463–473, 2009.

J. K. Guest, J. H. Prevost, and T. Belytschko. Achieving minimum length scale in topology optimization using nodal design variables and projection functions. *International Journal for Numerical Methods in Engineering*, 61(2):238–254, 2004.

R. B. Haber, C. S. Jog, and M. P. Bendsoe. A new approach to variable-topology shape design using a constraint on perimeter control. *Structural Optimization*, 11(1):1–12, 1996.

J. Haslinger and R. Makinen. *Introduction to Shape Optimization: Theory, Approximation and Computation*. Society for Industrial and Applied Mathematics, Philadelphia, PA, 2003.

X. Huang and Y. M. Xie. Optimal design of periodic structures using evolutionary topology optimization. *Structural and Multidisciplinary Optimization*, 36(6):597–606, 2008.

K. Ishii and S. Aomura. Topology optimization for the extruded three dimension structure with constant cross section. *JSME International Journal*, 47(2):198–206, 2004.

C. S. Jog and R. B. Haber. Stability of finite element models for distributed-parameter optimization and topology design. *Computer Methods in Applied Mechanics and Engineering*, 130(3–4):203–226, 1996.

J. Kim and G. H. Paulino. Isoparametric graded finite elements for nonhomogeneous isotropic and orthotropic materials. *ASME Journal of Applied Mechanics*, 69(4):502–514, 2002.

R. V. Kohn and G. Strang. Optimal design and relaxation of variational problems, Part I. *Communications on Pure and Applied Mathematics*, 39:1–25, 1986a.

R. V. Kohn and G. Strang. Optimal design and relaxation of variational problems, Part II. *Communications on Pure and Applied Mathematics*, 39:139–182, 1986b.

R. V. Kohn and G. Strang. Optimal design and relaxation of variational problems, Part III. *Communications on Pure and Applied Mathematics*, 39:353–377, 1986c.

L. Krog, A. Tucker, M. Kemp, and R. Boyd. Topology optimization of aircraft wing box ribs. *10th AIAA/ISSMO Multidisciplinary Analysis and Optimization Conference*, 2004.

C. Le. Achieving minimum length scale and design constraints in topology optimization: a new approach. Master's thesis, University of Illinois at Urbana-Champaign, 2006.

K. Matsui and K. Terada. Continuous approximation of material distribution for topology optimization. *International Journal for Numerical Methods in Engineering*, 59:1925–1944, 2004.

National Standard of the People's Republic of China, Code for Design of Concrete Structures, GB 50010-2002. Ministry of Construction of the People's Republic of China, 2002.

National Standard of the People's Republic of China, Code for Design of Steel Structures, GB 50017-2003. Ministry of Construction of the People's Republic of China, 2003.

K. Moon, J. J. Connor, and J. E. Fernandez. Diagrid structural systems for tall buildings: Characteristics and methodology for preliminary design. *The Structural Design of Tall and Special Buildings*, 16(2):205–230, 2007.

T. Nguyen, G. H. Paulino, J. Song, and C. Le. A computational paradigm for multiresolution topology optimization (MTOP). *Structural and Multidisciplinary Optimization*, in press, 2010.

T. Nomura, S. Nishiwaki, K. Sato, and K. Hirayama. Topology optimization for the design of period microstructures composed of electromagnetic materials. *Finite Elements in Analysis and Design*, 45(3):210–226, 2009.

G. H. Paulino, E. C. N. Silva, and C. Le. Optimal design of periodic functionally graded composites with prescribed propertiesn. *Structural and Multidisciplinary Optimization*, 38 (5):469–489, 2009.

J. Peterson and O. Sigmund. Slope constrained topology optimization. *International Journal of Numerical Methods and Engineering*, 41(8):1417–1434, 1998.

K. Qiu, W. Zhang, M. Domaszewski, and D. Chamoret. Topology optimization of periodic cellular solids based on a superelement method. *Engineering Optimization*, 41(3):225–239, 2009.

S. F. Rahmatalla and C. C. Swan. A Q4/Q4 continuum structural topology optimization implementation. *Structural and Multidisciplinary Optimization*, 27(1–2):130–135, 2004.

G. I. N Rovzany, M Zhou, and T. Birker. Generalized shape optimization without homogenization. *Structural Optimization*, 4:250–252, 1992.

G. I. N. Rozvany. Aims, scopes, methods, history and unified terminology of computer-aided topology optimization in structural mechanics. *Structural and Multidisciplinary Optimization*, 21(2):90–108, 2001.

G. I. N. Rozvany. A critical review of established methods of structural topology optimization. *Structural and Multidisciplinary Optimization*, 37(3), 2008.

U. Schramm, H. Thomas, and M. Zhou. Manufacturing considerations and structural optimization for automotive components. *Society of Automotive Engineers, Inc.*, 2002.

O. Sigmund. On the design of compliant mechanisms using topology optimization. *Mechanics of Structures and Machines*, 25(4):493–524, 1997.

O. Sigmund. Topology optimization: a tool for the tailoring of structures and materials. *Philosophical Transactions of the Royal Society*, 358(1765):211–227, 2000.

O. Sigmund. A 99 line topology optimization code written in matlab. *Structural and Multidisciplinary Optimization*, 21:120–127, 2001.

O. Sigmund. Morphology based black and white filters for topology optimization. *Structural and Multidisciplinary Optimization*, 33(4–5):401–424, 2007.

O. Sigmund and J. Petersson. Numerical instabilities in topology optimization: a survey on procedures dealing with checkerboards, mesh-independencies and local minima. *Structural Optimization*, 16:68–75, 1998.

L. L. Stromberg, G. H. Paulino, and W. F. Baker. Pattern Gradation and Repetition with Application to High-Rise Building Design. In *10th US National Congress on Computational Mechanics, Columbus, OH*, 2009.

K. Svanberg. The method of moving asymptotes: a new method for structural optimization. *International Journal for Numerical Methods in Engineering*, 24(2):359–373, 1987.

LEED® for New Construction & Major Renovations. U.S. Green Building Council, 2005.

M. Y. Wang and S. Wang. Bilateral filtering for structural topology optimization. *International Journal for Numerical Methods in Engineering*, 63(13):1911–1938, 2005.

W. Zhang and S. Sun. Scale-related topology optimization of cellular materials and structures. *International Journal for Numerical Methods in Engineering*, 68(9):993–1011, 2006.

M. Zhou and G. I. N. Rovzany. The COC Algorithm, Part II: Topological geometrical and generalized shape optimization. *Computer Methods in Applied Mechanics and Engineering*, 98(1-3):309–336, 1991.

M. Zhou and G. I. N. Rozvany. On the validity of ESO type methods in topology optimization. *Structural and Multidisciplinary Optimization*, 21(1):80–83, 2001.

M. Zhou, R. Fleury, Y. K. Shyy, H. Thomas, and J. M. Brennan. Progress in topology optimization with manufacturing constraints. *Proceedings of the 9th AIAA MDO Conference*, AIAA-2002-4901, 2002.

K. T. Zuo, L. P. Chen, Y. Q. Zhang, and J. Yang. Manufacturing- and machining-based topology optimization. *International Journal Advanced Manufacturing Technology*, 27(5–6):531–536, 2006.